

The Modeling of Partial Discharge under Fast, Repetitive Voltage Pulses Using Finite-Element Analysis

S. Moein R. Borghei

Dissertation submitted to the Faculty of the
Virginia Polytechnic Institute and State University
in partial fulfillment of the requirements for the degree of

Master of Science
in
Electrical Engineering

Mona Ghassemi, Chair
Vassilis Kekatos
Ahmad Safaai-Jazi

April 15, 2020
Blacksburg, Virginia

Keywords: Fast-rise square wave voltages; finite-element analysis; high frequency;
insulation systems; partial discharge modeling.

Copyright 2020, S. Moein R. Borghei

The Modeling of Partial Discharge under Fast, Repetitive Voltage Pulses Using Finite-Element Analysis

S. Moein R. Borghei

(ABSTRACT)

By 2030, it is expected that 80% of all electric power will flow through power electronics systems. Wide bandgap power modules that can tolerate higher voltages and currents than silicon-based modules are the most promising solution to reducing the size and weight of power electronics systems. These wide-bandgap power modules constitute powerful building blocks for power electronics systems, and wide bandgap-based converter/power electronics building blocks are envisaged to be widely used in power grids in low- and medium-voltage applications and possibly in high-voltage applications for high-voltage direct current and flexible alternating current transmission systems. One of the merits of wide bandgap devices is that their slew rates and switching frequencies are much higher than silicon-based devices. However, from the insulation side, frequency and slew rate are two of the most critical factors of a voltage pulse, influencing the level of degradation of the insulation systems that are exposed to such voltage pulses. The shorter the rise time, the shorter the lifetime. Furthermore, lifetime dramatically decreases with increasing frequency. Thus, although wide bandgap devices are revolutionizing power electronics, electrical insulating systems are not prepared for such a revolution; without addressing insulation issues, the electronic power revolution will fail due to dramatically increased failure rates of electrification components. In this regard, internal partial discharges (PDs) have the most effect on insulation degradation. Internal PDs which occur in air-filled cavities or voids are localized electrical discharges that only partially bridge the insulation between conductors. Voids in solid or gel dielectrics are

challenging to eliminate entirely and may result simply during manufacturing process. The objective of this study is to develop a Finite-Element Analysis (FEA) PD model under fast, repetitive voltage pulses, which has been done for the first time. The model is coded and implemented in COMSOL Multiphysics linked with MATLAB, and its simulation results are validated with experimental tests. Using the model, the influence of different parameters including void shape, void size, and void air pressure on PD parameters are studied.

The Modeling of Partial Discharge under Fast, Repetitive Voltage Pulses Using Finite-Element Analysis

S. Moein R. Borghei

(GENERAL AUDIENCE ABSTRACT)

To decarbonize and reduce energy consumption for commercial aviation, the development of lightweight and ultra-efficient all-electric powertrain including electric motors, drives, and associated thermal management systems has been targeted. Using wide bandgap (WBG) power modules that can tolerate high voltages and currents can reduce the size and weight of the drive. However, the operation of WBG-based power converter can endanger the reliability of the electrified systems, most importantly, the insulation system. In this study, it is attempted to model the impact of such threats to the insulation system using numerical models.

Dedication

I dedicate my dissertation work to my family and many friends. A special feeling of gratitude to my loving parents, Hossein and Mansoureh whose words of encouragement and push for tenacity ring in my ears. Also, my brother, Mohammadreza, who has never left my side.

Acknowledgments

I wish to thank my committee members who were more than generous with their expertise and precious time. A special thanks to Dr. Mona Ghassemi, my committee chairman and advisor for her profound support and countless hours of reflecting, reading, encouraging, and most of all patience throughout the entire process. Thank you Dr. Vassilis Kekatos, and Dr. Ahmad Safaai-Jazi for agreeing to serve on my committee.

Publications

- M. Borghei, M. Ghassemi, J. M. Rodriguez-Serna, and R. Albarracin-Sanchez, "A Finite-Element-Analysis and an Improved Induced Charge Concept for Partial Discharge Modeling", *IEEE Transaction on Power Delivery*, 1st round of revision.
- M. Borghei, M. Ghassemi, "A Finite Element Analysis Model for Partial Discharges in Silicone Gel under a High Slew Rate, Frequency Square Wave Voltage in Low-Pressure Conditions", *Energies*, *Accepted*.
- M. Borghei, M. Ghassemi, "Partial Discharge Analysis under High-Frequency, Fast-Rise Square Wave Voltages in Silicone Gel: A Modeling Approach", *Energies*, vol. 12, no. 23, 2019.
- M. Borghei, M. Ghassemi, "Finite Element Modeling of Partial Discharge Activity within a Spherical Cavity in a Solid Dielectric Material under Fast, Repetitive Voltage Pulses", *IEEE Electrical Insulation Conference (EIC)*, Calgary, Canada, June 2019.
- M. Borghei and M. Ghassemi, "Partial Discharge Finite Element Analysis under Fast, Repetitive Voltage Pulses," *2019 IEEE Electric Ship Technologies Symposium (ESTS)*, Washington, DC, USA, 2019, pp. 324-328.
- M. Borghei, M. Ghassemi, "The Influence of Frequency of Fast, Repetitive Voltage Pulses from WBG Power Electronics on Partial Discharges under Low-Pressure Conditions", *2020 IEEE Energy Conversion Congress Expo (ECCE)*, *Accepted*.

Contents

List of Figures	xi
List of Tables	xiii
1 Introduction	1
1.1 Background	1
1.2 Motivation	3
1.3 Objective	5
1.4 Outline	7
2 Theories on PD Phenomenon	8
2.1 PD Types	8
2.2 PD Models	9
2.3 PD Mechanism	10
2.4 PD Inception and Extinction	12
2.5 Initial Electron Generation	13
2.6 PD Memory	15
2.7 Summary	16

3	PD Modeling	17
3.1	Streamer Inception Criterion	17
3.2	PD Extinction	18
3.3	Initial Electron Generation	19
3.3.1	Physics-based Representation	20
3.3.2	Experimental-based Representation	24
3.3.3	Probability of PD occurrence	25
3.4	PD Transient State	26
3.4.1	Conductive State of PD	26
3.4.2	Charge Calculation	27
3.5	Charge Decay	28
3.6	Algorithm	31
3.7	Summary	33
4	Numerical Results	34
4.1	Case Studies	34
4.1.1	Case 1:	34
4.1.2	Case 2:	37
4.2	Electric Field Distribution	40
4.3	PD Charge Magnitude	42

4.4	Impact of Cavity Characteristics	44
4.4.1	Cavity Diameter	44
4.4.2	Cavity Location	46
4.4.3	Cavity Shape	47
4.5	Impact of Applied Voltage Parameters	48
4.6	Impact of Pressure	49
4.7	Key Challenges	53
4.7.1	Estimation of Model Parameters	53
4.7.2	Convergence Problem	55
4.7.3	Burden of Calculation	56
4.7.4	Dielectric Constant (relative permittivity)	58
4.8	Summary	60
5	Conclusions	62
5.1	Discussion and Inference	62
5.2	Future Works	63
	Bibliography	65

List of Figures

2.1	PD Types: (a) internal discharge, (b) surface discharge, and (c) corona. . . .	8
2.2	Streamer formation between two electrodes [1]	11
2.3	Initial electron generation sources.	14
3.1	Movement of particles when (a) polarity does not change, and (b) polarity changes.	22
3.2	PD modeling flowchart.	32
4.1	3D representation of 1st case study.	34
4.2	2D representation of 1st case study.	35
4.3	Mesh pattern of 1st case study.	37
4.4	3D representation of 2nd case study.	37
4.5	2D representation of 2nd case study.	38
4.6	Mesh pattern of 2nd case study.	40
4.7	The whole system electric field distribution before PD occurrence.	40
4.8	The whole system electric field distribution after PD occurrence.	41
4.9	Axial electric field distribution after PD occurrence.	41
4.10	Radial electric field distribution after PD occurrence.	42
4.11	Electric field distribution in 2nd case.	43

4.12	PRPD pattern for 1st case study.	44
4.13	PRPD pattern for 2nd case study.	45
4.14	Effect of diameter on electric field magnitude in 1st case.	46
4.15	Impact of voltage shape.	47
4.16	Impact of cavity diameter on PD charge magnitude.	48
4.17	Impact of cavity diameter on PD charge magnitude.	49
4.18	PD inception voltage as a function of location in r-axis.	50
4.19	PD inception voltage as a function of location in z-axis.	50
4.20	Impact of cavity shape on inception voltage.	51
4.21	The impact of cavity shape on PD charge magnitude	52
4.22	The frequency impact on PD inception	53
4.23	The impact of cavity shape on PD charge magnitude	54
4.24	The impact of cavity shape on PD charge magnitude	55
4.25	Impact of pressure on inception and extinction electric field.	56
4.26	PD inception time as a function of pressure.	56
4.27	The relation between pressure and PD duration.	57
4.28	The PD charge magnitude versus pressure.	57
4.29	The 3D PRPD Pattern for the case study after 50 cycles.	58
4.30	The impact of compaction technique on calculation burden.	59
4.31	The variations of relative permittivity with pressure.	60

List of Tables

4.1	Geometrical Parameters of 1st Case	35
4.2	Square Wave Voltage Parameters for 1st Case	36
4.3	Mesh Properties of 1st Case	36
4.4	PD Parameters for 1st Case	36
4.5	Geometrical Parameters of 2nd Case	38
4.6	Square Wave Voltage Parameters for 2nd Case	38
4.7	Mesh Properties of 2nd Case	39
4.8	PD Parameters for 2nd Case	39
4.9	PD Results for 1st Case	43
4.10	PD Results for 2nd Case	44

Chapter 1

Introduction

1.1 Background

As air quality has kept becoming a more and more vital problem in 21st century, electrification of various systems and equipment has been offered as a solution to that [2]. The rapid growth of electrification also lies in several other advantages of using electricity over conventional energy resources. These advantages include the more flexibility and controllability that electric systems provide, also the transmission of power at almost the speed of light and the capability of electricity to be stored give more merits to this trend [3].

The electrification trend initiated in the transportation section, specifically in electric cars and it keeps moving toward the naval and aviation industry. Annual global growth of 4.7% is expected until 2028 in the commercial air traffic demand, also doubling the number of passengers in the upcoming 20 years till 2040 [4, 5]. On the other hand, economic and environmental problems should be overcome to facilitate electrification in these sectors. As it is reported in [6], the commercial aviation consumed almost 16% of the total petroleum (crude oil and products) imports of the US. In the same year, 2.6% of domestic greenhouse gas emissions (174.8 million metric tons of CO_2) was produced by air travels [7]. To address the above issues, i.e. energy consumption and carbonization, electrified aircraft technologies have been aimed.

Besides, by the end of 2030, it is expected that 80% of power will flow through power electronics employed across the power grid [8]. Rapid-growing penetration of power electronics into various residential, industrial, and commercial levels by integration of more renewable energy into power grid emphasizes on the key role played by power electronics systems in future smarter grid, expanded from transmission to distribution, and furtherly to the consumers [9, 10, 11]. Power electronics also has a substantial role in transferring energy from electric energy storage systems to the electrical grid and vice versa [12]. Furthermore, bidirectional dc chargers, FACTS devices are some other power electronics technologies being developed [13].

In modern converters, the emergence of WBG-based systems has led to significantly high efficiencies. Moreover, maturity of these WBG semiconductor technology in the next generations of power electronic modules has enabled them to operate at higher voltages, higher frequencies, and higher temperatures [14]. Commercially, these new highly efficient devices are being more and more available [15]. Although WBG-based converters have an electric breakdown about 10 times higher than silicon (Si)-based systems[16], the operation at of these devices at high frequencies (50 kHz and above) can cause the rapid deterioration of insulation systems through intensive electric stress. Various methods of insulation health diagnosis are found including partial discharges, leakage current, electrical breakdown, dielectric losses, and electric field distribution [17].

Among the different degradation mechanisms, the accelerated aging of insulation systems due to fast, repetitive voltage pulses originated by WBG-based converters can be mentioned as the major obstacle toward employment of this technology [18]. The most crucial insulation degradation factor under fast, repetitive voltage pulses is PD [19, 20].

According to IEC 60270, PDs are local electrical discharges that do not completely bridge the insulation between conductors and may or may not occur adjacent to a conductor. If the

electric field intensity across a portion of dielectric exceeds its electrical breakdown strength, then a local breakdown is expected. This phenomenon is known as partial breakdown or partial discharge (PD). The charged particles (electrons, positive ions, and negative ions) produced during the discharge move toward the void's wall and, subsequently erode the dielectric through bombardment of the wall. Secondary electrons can, then, be generated through these collision as a function of dielectric's work function. Moreover, the discharge can give rise to some products such as O_3 or NO_2 , which further causes chemical degradation of the solid dielectric. Thus, despite the fact that PD does not impose a global breakdown between electrodes, the slow deterioration of dielectric material can eventually cause the breakdown of solid dielectric [21, 22].

1.2 Motivation

Although numerous techniques have been evolved to detect and localize PDs [23, 24, 25], PD modeling has not reached the same end. Among different studies performed on PD modeling, the modeling of cavity-dielectric system gained the most attention, starting in the early 19th century [26, 27, 28]. The major concentration of these studies has been on PD analysis and quantification under sinusoidal waves; however, the growing penetration of power electronics into power grid has substantiated the need to study PD under fast, high-frequency square wave (PWM-like) pulses.

Among the studies conducted on PD phenomenon so far, major works have focused on understanding the effect of the existence of a void within the dielectric [26, 27, 28, 29]. The formation of cavities and air-filled bubbles is natural during the manufacturing process of dielectrics while the streamer propagation can also lead to formation voids [30, 31]. Al-

though the emergence of the Vacuum Pressure Impregnation (VPI) technique has lowered the number and volume of cavities inside the insulating medium, making it zero does not seem a plausible mission. In [32], it is revealed that the electrical treeing is another reason to the existence of cavities. Although some studies have confirmed that some dielectrics have self-healing capability, this is not the case for a lot of insulating materials such as silicone gel which is the predominant encapsulating material in power electronics. In silicone gel, a cavity can remain up to 10 ms that is 1000 times higher than non-viscous liquids [33] which causes the gradual deterioration of insulating material.

Since the permittivity of the gas (air, SF₆, etc.) is usually less than the dielectric's permittivity, the voids are called weak points due to the higher electric field across the cavity higher than the dielectric. In [34], it is shown that the electric field intensity in a spherical void is about 30% higher than the case of void-free dielectric. Therefore, the examination of cavity effect on the health of dielectric must be performed.

Frequency and rise time are among the most destructive factors of a square wave voltage [35]. Thus, although WBG-based power electronics can present higher power density, voltage pulses having extremely high slew rate and frequencies can introduce severe threats to the health of insulation systems in WBG power modules [36, 37], where the breakdown can happen within hours or even minutes [35]. Although geometrical techniques or using nonlinear resistive grading coating layers can help lowering the electric field intensity [36, 38, 39], it is still necessary to understand the mechanisms behind PD can help to better implement electric field control methods. Another strategy one might bring up is the adoption of a thicker layer of dielectric; however, this cannot be a promising solution due to the tremendous desire of power electronics industry for miniaturization [40, 41, 42].

Moreover, it has been reported through experimental investigations that the fast-rise, high-frequency square wave voltages have a detrimental impact on the health of dielectrics in

terms of PD ignition rate and intensity [43, 44]. In [45], the detrimental impacts of a high slew rate were studied, and the results showed that high slew rate square voltages substantially increased the intensity of PDs within the insulating medium and changed the PD spectrum. It has also been shown in [46, 47] that, although at a higher frequency the PD intensity is lower, the higher repetition rate causes rapid degradation of insulation. Thus, at higher frequencies, the lifetime of insulation is reduced. All the challenges mentioned in this section demonstrate the prominence of a profound investigation into the PD phenomenon as the insulation system puts a limiting factor on the reliability of the whole system.

1.3 Objective

Various models have been proposed for the modeling of PD using the cavity-dielectric representation [48, 49, 50, 51, 52, 53, 54]. In this study, the FEA method is used to dynamically model the PD phenomenon. The advantage of FEA over other models is its ability to apply to sophisticated geometries as well as its ability to dynamically monitor changes in the values of electrical properties such as electric field, current density, field displacement, etc. [55]. The parameters associated with the FEA are selected such that the results meet experimental reports in the literature.

The goal of this study is to explore the PD phenomenon and its characteristics under high-frequency, fast-rise square wave voltage on which insufficient work has been conducted. In this case, two PDs take place for each pulse: one on the rising flank, and the other on the falling one. The various parameters in the study of PD under repetitive voltage pulses includes but is not limited to frequency, rise time, and amplitude of the applied voltage.

To model PD phenomenon, one should bear in mind that PD is a stochastic process and

can be controlled by various factors concerning the physical processes. For instance, the location and shape of the voids have a substantial impact in PD inception [21]. Considering all these conditions, it is aimed to find the variation of PD magnitude with respect to different parameters that are assessed by the FEA model developed in this study. These parameters can include void characteristics such as size and shape. They also constitute environmental and electrical specifications such as air pressure inside the void, temperature, and void conductivity.

Besides the importance of delving into the stochastic property of PD events to obtain an accurate PD pattern, it is also important to investigate the physics of PD phenomenon. In order to provide a valid comparison among different values for a given parameter, the stochastic property of PD should be frozen. The reason for this is that the variations of the random nature of PD can significantly influence the physical meaning of the outcome, misleading our judgment about a certain parameter.

Aside from the impact of the applied voltage characteristics, environmental conditions can also change the way the PD phenomenon is looked at today. For instance, an aircraft can be at a pressure as low as 4 psi when flying at cruising altitude where the impact of pressure on PD occurrence has not been sufficiently studied so far. To the best of author's knowledge, there is only one paper reporting experimental investigations on the effect of fast, repetitive voltage pulses (5 to 200 kHz) at pressure levels between 20 and 100 kPa on repetitive partial discharge inception voltage (RPDIV) of a solid dielectric (a twisted wire pair) [56].

This study also focuses on the effects that low-pressure conditions have on different model parameters and reflects on how these changes affect PD characteristics. The work was done under high frequency, high slew rate voltages to accurately model the escalated tension that the insulation system undergoes.

1.4 Outline

In chapter 2, the theories for the PD phenomenon are reviewed. First, PD types are introduced and then, the models for PD analysis are discussed. After that, the physical mechanism of PD is explained and an overview of the theories for PD inception, extinction, and initial electron generation is presented. Finally, the concept of PD memory is discussed.

In chapter 3, the theories introduced in chapter 2 are mathematically presented. At first, the streamer inception criterion and the condition for PD quenching are presented. Then, different theoretical and experimental representations of initial electron generation are overviewed. Later in this chapter, the charge decay process and calculation procedure of PD charges are discussed. Finally, the whole algorithm for PD analysis is developed.

In chapter 4, the two case studies that are used for the evaluation of the proposed algorithm are introduced. Then, the electric field distribution in each of these case studies is obtained with the aid of FEA. Then, the PRPD pattern for each case is obtained, and also the impact of cavity properties is assessed on PD events. After that, the influence of applied voltage characteristics on the PD phenomenon is evaluated. Finally, the performance of insulation under extremely low-pressure conditions is examined.

In chapter 5, the conclusions and future works are brought, and the references are listed in the last section.

Chapter 2

Theories on PD Phenomenon

2.1 PD Types

PDs can occur in solids, liquids, and gases and are usually divided into three groups (shown in Fig. 2.1). The PDs occurring in the cavities or inclusion inside a solid or liquid dielectric are called “Internal Discharges” (see Fig. 2.1(a)). This type of PDs is usually inevitable as it is part of the manufacturing process in the case of solid and liquid insulating mediums. Examples of internal discharges include but not are limited to the PDs occurring in the transformer oils, or inside the silicone gel which encapsulates a power converter. If PD

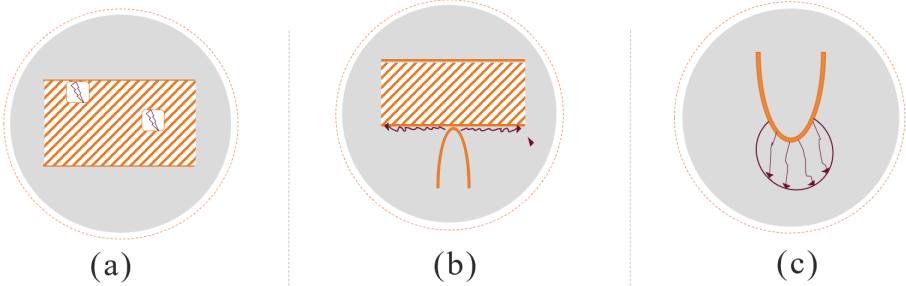


Figure 2.1: PD Types: (a) internal discharge, (b) surface discharge, and (c) corona.

occurs at the interface between air (or any other gaseous medium) and a liquid or solid dielectric, it is called “Surface Discharges” (see Fig. 2.1(b)), also known as “tracking”. This usually occurs when the electric field component parallel to the interface goes extremely high [1]. Instances of surface discharge include discharges at the interface of bushings, cable

terminations, and insulators.

Under a strongly inhomogeneous electric field around an electrode, a local and continuous breakdown can happen which is known as “Corona” (see Fig. 2.1(c)). A famous example of corona can be found near high-voltage transmission lines which are coupled with constant noise and a glow of light that is observable in darkness. The mentioned effects are due to the constant ionization of air under the intense electric field.

2.2 PD Models

To date, four major PD models are introduced to represent a cavity-dielectric system; in the order of their introduction date, the models are three-capacitance (abc), induced charge concept (ICC), finite element analysis (FEA), and Multiphysics models. The abc-model firstly introduced by Whitehead [48] used an equivalent circuit including three capacitances to model the cavity, the insulation in series with the cavity, and the remaining insulation. While being a relatively simple model, it gives a proper insight into PD mechanism from a macroscopic point of view. However, the inability of the model to validly represent physics behind PD has been enumerated as one of the major disadvantages of this model [49].

Pedersen et al. later proposed an analytical model in which the concept of induced charge on the electrode was used to explain the partial discharge transients [49, 50, 51]. While analytical model gave more explanations on the physical process behind PD, it could be too complicated to be applied to more sophisticated geometries. Moreover, the assumptions made for simplification have aroused serious questions on the validity of the model; for example, the assumption that system’s capacitance remains unaffected by PD later rejected in [53].

On the other hand, although Multiphysics models [57, 58] may be able to accurately model mechanisms and phenomena associated with PDs, there are many physical parameters in the model that need to be experimentally determined. Adjusting these physical parameters to meet PD measurements for a specific testing geometry and dimension cannot always be generalized.

The availability of advanced computational tools have enabled the utilization of numerical methods including Finite Difference Method (FDM), Finite Element Method (FEM), and Charge Simulation Method (CSM) [59]. Using these methods, one can numerically estimate the electric field intensity in the cavity-dielectric system. As will be shown later, almost all the aspects of PD phenomenon are related to electric field distribution and intensity; therefore, an accurate estimate of the electric field can pave the road for understanding and quantification of the PD characteristics. Thanks to the availability of power computational systems, this study takes advantage of FEA to investigate the PD phenomenon.

2.3 PD Mechanism

Prior to occurrence of a PD, the electric field ought to exceed the inception electric field to initiate the electron avalanche. Another prerequisite is that at least a free electron should exist for initiation of ionization process. These conditions will be deeply explored later in this section.

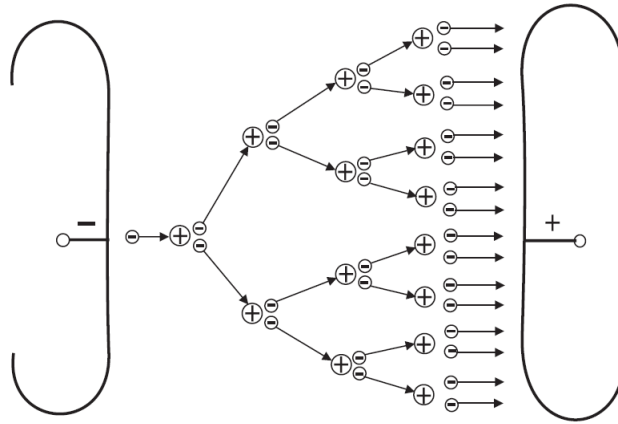


Figure 2.2: Streamer formation between two electrodes [1]

The occurrence is accompanied by the movement of charged particles, e.g. electrons and ions (Fig. 2.2). These charged particles are resulted by the collisions among accelerated electrons and the other atoms/molecules. In high-intensity electric field region, the free electrons can accelerate and collide with other particles to further produce electrons and positive ions. This process is called electron avalanche and can happen only when the two above conditions are met.

Once the above conditions are met, the discharge takes place through an increase in the value of cavity conductivity. The lower the electrical resistance of the cavity is, the higher the electric field goes inside the cavity. The ionization that occurs during the discharge leaves charged particles on the cavity surfaces (true PD charge), also inducing charge on the electrodes (apparent PD charge). The discharge continues to grow until the ionization process halts. The ionization only stops when the electrons do not have enough energy to collide with further atoms/molecules and ionize them. The electric field at which the electron avalanche can no longer grow is known as the “extinction electric field”. Both the inception and extinction fields can also be described as the potential difference instead of the electric field.

Among the two types of charges that can be detected for a partial discharge event, only apparent charge magnitude is measurable as the current flowing through the cavity cannot be measured with the typical experimental setup. The merit that goes to simulation methods is that they can provide the opportunity to also estimate the true charge magnitude aside from the apparent charge.

2.4 PD Inception and Extinction

A PD does not completely bridge between the electrodes; however, in this case, a local discharge occurs in the defects or cavities within the insulating medium. A PD takes place once a free electron is provided and it is sufficiently energetic to ionize further atoms or molecules and causes the growth of streamer, as demonstrated in Fig. 2.2.

Therefore, for being able to correctly predict the time at which PD initiates, an accurate estimation of electric field magnitude at which ionization process starts is required. To achieve so, a critical avalanche criterion has been suggested in [49] that investigates the critical number of electrons required to have a self-propagating avalanche [34]. The following equation expresses the streamer inception criterion:

$$\frac{E_{inc}}{E_{cr}} = F \quad (2.1)$$

The relationship between PD inception field and breakdown critical field is described by a dimensionless parameter, F , that is dependent on gas filling the cavity, dielectric constant, and the defect geometry. It can be defined for a spherical void as follows:

$$F = 1 + \frac{B}{(pd)^n} \quad (2.2)$$

where B , and n are gas-related constants. The other parameters are gas pressure p , and void diameter in the direction of background field d .

One should not forget the impact of environmental conditions such as humidity that decreases the breakdown field of dielectrics [60].

2.5 Initial Electron Generation

Another condition for PD occurrence is that the existence of initial electrons for the ionization process must be ensured. There are two processes, volume ionization and surface emission, for the generation of initial electrons in the void. Each includes the following mechanisms [34]. Thus, the total rate of the generation of initial electrons per unit of time can be

Surface Emission

- I Detrapping of electrons from the surface of the insulator
- II Electron emission by photo effect from the surface of the insulator
- III Unleashing electrons by ion impact
- IV Electron emission by photo effect from the surface of the conductor
- V Electron release from the conductor due to the electric field

Volume Ionization

- VI Gas ionization by irradiation of energetic photons
 - VII Detachment of electrons from negative ions due to field intensity
-

expressed as the summation of the electron generation rates due to each of the processes:

$$\dot{N}_{tot}(t) = \dot{N}_{surf}(t) + \dot{N}_{vol}(t) \quad (2.3)$$

where $\dot{N}_{surf}(t)$ is the electron generation rate due to surface emission and $\dot{N}_{vol}(t)$ quantifies the contribution of the volume ionization. In the following parts, each of these processes are delineated in detail. In surface emission, electrons are emitted from the void surface by

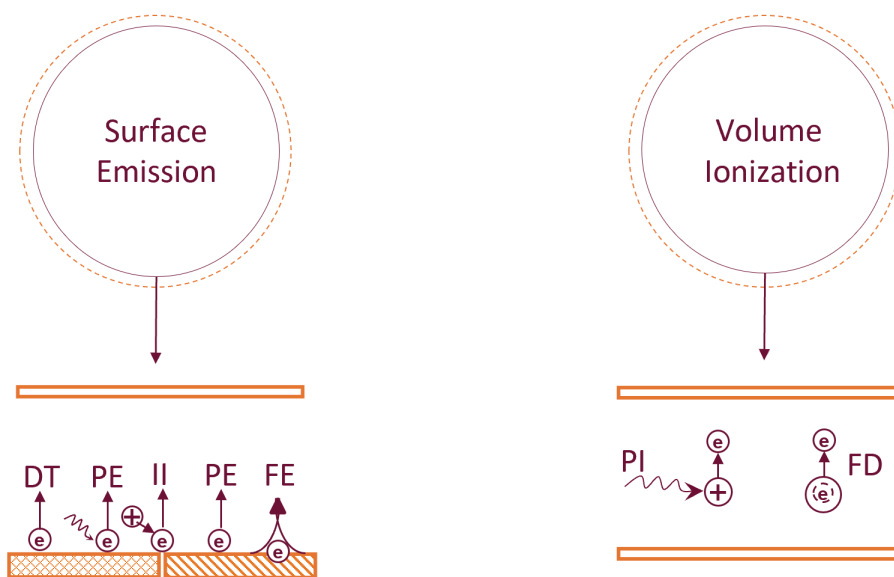


Figure 2.3: Initial electron generation sources.

mechanisms I through V. The dominating mechanism of surface emission is the detrapping of electrons accumulated on the surface of the void [34], which is dependent upon the electric field and the temperature inside the void. Thus, the electron generation rate due to the surface emission process can be fitted to Richardson-Schottky scaling given by [61, 62, 63].

While some studies have neglected the contribution of volume ionization owing to a lower rate of electron generation compared to surface emission [57, 64, 65], volume ionization is the dominant provider of free electrons in some cases. There might be some times at which

free electrons cannot be supplied from surface emission mechanisms such as is the case of the first PD event. At the first PD event, no electron is available to be detrapped from the void wall; thus, volume ionization plays a significant role. As the rate of electron generation due to volume ionization is much lower than the surface emission, there is a considerable inception delay time before the occurrence of the first PD. Volume ionization might occur due to the irradiation of energetic photons (mechanism VI) or field detachment of electrons from negative ions (mechanism VII) [34].

2.6 PD Memory

The charges remained from previous PD events do not last infinitely; however, the induced charges can have an impact on the upcoming PD events in two ways: (1) they will affect the electric field distribution across the cavity, and (2) they provide an additional source for the initial electron generation that is a must for the next PD events. Therefore, as the PD events memory will remain in effect until a period of time, this effect is known as “PD memory”.

The impact of PD memory is mainly influenced by the decay rate of the produced PD charges. There are three mechanisms for charge decay:

(1) Space charge decay through ambipolar ion drift (2) Surface charge decay through ion drift (3) Surface charge decay through surface conduction The above mechanisms can give rise to another electric field component (internal field) other than the main component which is due to the applied voltage (external field). The internal field component can sum up to the external field or vice versa. Depending on each of these scenarios, the statistical time lag for the ignition of the next PD event can be affected.

2.7 Summary

In this chapter, the theories behind PD were discussed. In the first place, different PD types are introduced and the examples of each type were brought. Then, four major models for PD analysis were reviewed and the advantages and disadvantages of each model were examined. Thereafter, the mechanism of PD through the change in the value of cavity conductivity was discussed. It was shown that the two conditions must be satisfied in order to have a discharge. One is the existence of an initial free electron which can be provided either through surface emission or volume ionization. The second condition was that the electrons should have sufficient energy to cause electron avalanche. Finally, the PD memory effect was introduced. This effect simply means that a PD event that induces charges on the cavity wall and on the electrodes, can have an impact on the upcoming PD events.

In the next chapter, the theories discussed in this chapter will be mathematically formulated.

Chapter 3

PD Modeling

3.1 Streamer Inception Criterion

For a PD to begin, two conditions should be met; first, the electric field across the cavity ought to exceed the PD inception field (E_{inc}) and secondly, at least one free electron must be there to give rise to the ionization process. Therefore, a necessary condition is the critical avalanche criterion [66, 67]:

$$\int_0^{x_{cr}} \bar{\alpha}[E(x)]dx \geq K_{cr} \quad (3.1)$$

where $E(x)$ represents the electric field magnitude along the streamer path, K_{cr} is the logarithm of electrons needed at the avalanche head to have a self-propagating avalanche. $\bar{\alpha}$ stands for the effective Townsend ionization coefficient, and finally, x_{cr} is the length of the streamer path. In [49], the aforementioned inequality is simplified into the following conditions for an ellipsoidal void:

For an electron attaching gas (such as SF6):

$$\frac{E_{inc}}{p} = \left(1 + \frac{M}{2ap}\right) \left(\frac{E}{p}\right)_{cr} \quad (3.2)$$

For a non-attaching gas (such as air):

$$\frac{E_{inc}}{p} = \left(1 + \frac{B}{(2ap)^n}\right) \left(\frac{E}{p}\right)_{cr} \quad (3.3)$$

where p is gas pressure and a is the radius of the ellipsoidal void parallel to the background field. B and $(\frac{E}{p})_{cr}$ are gas-related parameters for the ionization process. M is the figure of merit for the attaching gas and is defined in [49] as a function of $(\frac{E}{p})_{cr}$.

For air, the values of $(\frac{E}{p})_{cr}$ and B are $24.2 \text{ VPa}^{-1} \text{ m}^{-1}$ and $8.6 \text{ Pa}^{1/2} \text{ m}^{1/2}$.

3.2 PD Extinction

Discharge occurs through an increase in the cavity conductivity from an initial value (approximately zero) to a higher value $\sigma_{cav,max}$. An increase in conductivity results in a decrease in the electric field intensity inside the cavity. Conductivity remains at a high value until the electric field recedes to a certain magnitude, called the Extinction Electric Field (E_{ext}). According to Gutfleisch and Niemeyer [34, 52], the electric field at which PD is quenched can be described as a function of the critical electric field:

$$E_{ext} = \gamma p \left(\frac{E}{p} \right)_{cr} \quad (3.4)$$

In the above expression, γ is a dimensionless factor varying with the change of voltage polarity. γ can be estimated experimentally. This work determines γ such that at normal temperature and pressure (NTP) conditions (p_0, T_0) , E_{ext} equals the value proposed in the literature.

3.3 Initial Electron Generation

The other condition aside from streamer inception criterion probes into the existence of at least one initial free electron necessary for a discharge to happen. Hence, a statistical time delay is still expected even once the inception field condition is met.

As mentioned earlier, a free electron is necessary for the development of the electron avalanche. To quantify this condition, a function is required which stands for the rate of electron generation. Generally speaking, there are two main sources for production of the initial electrons: Volume generation, and surface emission [34].

In the case of volume ionization, the beam of highly-energetic photons could produce of electrons along with the electrons detached from negative ions owing to the electric field impact. In the surface emission, the cathodic conductors might release free electrons or the detrapping of previous PD electrons from the insulator surface.

While Niemeyer used the above physical processes to define the electron generation rate, Forssen [65, 68], and later Illias [64, 67, 69] utilized a simplified model which is accordance

with experimental data.

In the simplified representation, the total electron generation rate, $\dot{N}_{tot}(t)$, consists of two components. One is the electron generation rate due to surface emission $\dot{N}_{surf}(t)$, and the other is the electron generation rate due to volume ionization $\dot{N}_{vol}(t)$:

$$\dot{N}_{tot}(t) = \dot{N}_{surf}(t) + \dot{N}_{vol}(t) \quad (3.5)$$

3.3.1 Physics-based Representation

- **Surface Emission**

In surface emission, electrons are emitted from the void surface by mechanisms I through V mentioned in Section 2.5. The dominating mechanism of surface emission is the detrapping of electrons accumulated on the surface of the void [70], which is dependent upon the electric field and the temperature inside the void. Thus, the electron generation rate due to the surface emission process $\dot{N}_{surf}(t)$ fitted to Richardson-Schottky scaling given by [34, 52, 70]:

$$\dot{N}_{surf}(t) = N_{surf} \nu_0 \exp\left(-\frac{\phi - \sqrt{\frac{eE_{cav}(t)}{4\pi\epsilon_0}}}{kT}\right) \quad (3.6)$$

where $\nu_0 \approx 10^{13} - 10^{14} s^{-1}$ [34] is the fundamental phonon frequency of the material (for epoxy resin $\nu_0 \approx 10^{14} s^{-1}$ [52]). The effective detrapping work function of the material, ϕ , is in eV units, and e is the elementary charge of the electron. The surface emission rate can sensitively change with respect to the value of ϕ [34]. E_{cav} is the electric field intensity inside the void due to surface charges on the void wall, $\epsilon_0 = 8.854 \times 10^{-12} F.m^{-1}$ is the vacuum permittivity, $k = 8.6174 \times 10^{-5} eV.K^{-1}$ is Boltzmann's constant, and T is the absolute temperature. N_{surf} is the number of electrons

available to be detrapped from the void surface for the next PD. In [70] it was assumed that the total true physical charge of the previous PD, q , can participate in the detrapping mechanism and, thus, N_{surf} was approximated by q/e . However, it was assumed in [34, 52] that this number is affected by two factors delineated below. The first factor, known as the proportionality factor (ξ), describes the fraction of the charge carriers that result in the creation of detrappable electrons. The contribution of this factor denoted as N_{surf0} is given by

$$N_{surf0} = \xi \frac{q}{e} \quad (3.7)$$

where $\xi < 1$. In Figure 3.1, the movement of charged particles is shown under two different conditions. The electric field due to the applied voltage ($E_{app}(t)$) is one of the two components of the electric field inside the void. However, owing to the lower permittivity of the gas inside the void than that of the solid dielectric, the magnitude of $E_{app}(t)$ is multiplied by an enhancement factor (f) that quantifies the intensification of $E_{app}(t)$ inside the void. The derivation of f will be discussed later in (17). Aside from $fE_{app}(t)$, the electric field inside the void includes another component, called $E_{int}(t)$, which is the electric field due to surface charges remaining on the surface of the void from the previous PD events. The summation of these two components yields the net electric field magnitude inside the void ($E_{cav}(t)$). The demonstration of the movement of charged particles in the void when the direction of the electric field between two consecutive PDs (a) does not change, (b) changes. In Figure 3.1a, the direction of $E_{app}(t)$ remains constant between two consecutive PDs and the charged particles move in the opposite direction. On the other hand, when the direction of $E_{app}(t)$ changes between two consecutive PD events, the directions of the two field components would be the same. Thus, the positive ions and electrons approach each other (Fig. 3.1 b).

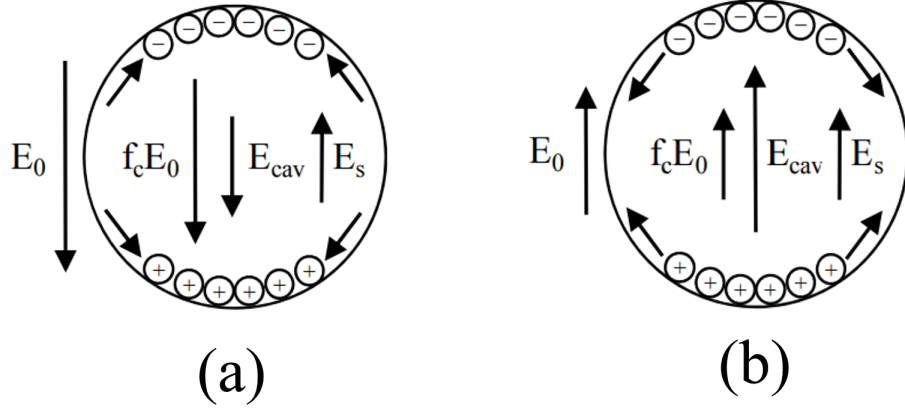


Figure 3.1: Movement of particles when (a) polarity does not change, and (b) polarity changes.

Due to the neutralization of the charged particles, the number of available electrons for the upcoming PD event is reduced. Therefore, a global value for the proportionality factor (ξ) may not provide an accurate explanation for the estimation. When the polarity of electric field changes between two consecutive events, the electron detrapping mechanism is much more difficult from a negatively charged void surface than the case of a positively charged one. To distinguish these two scenarios, ξ_+ and ξ_- are defined for positively and negatively charged void surfaces, respectively. As the second factor, while N_{surf0} electrons are expected to accumulate on the void wall, it is also expected that these electrons decay during the time intervals between events. The decay processes may cause the electrons in the shallow traps to hop into deeper ones, from which it is very hard to be detrapped. The electrons might also become inactive in PD ignition by diffusing into the depth of insulating medium. Considering the influence of the two factors, N_{surf} is given by [34, 52]:

$$N_{surf} = N_{surf0} \exp\left(-\frac{t}{\tau_{decay}}\right) \quad (3.8)$$

where t is the time passed from the last PD event and τ_{decay} is the decay effective time constant.

- **Volume Ionization**

While some studies have neglected the contribution of volume ionization owing to a lower rate of electron generation compared to surface emission [57, 64, 65], volume ionization is the dominant provider of free electrons in some cases. There might be some times at which free electrons cannot be supplied from surface emission mechanisms such as is the case of the first PD event. At the first PD event, no electron is available to be detrapped from the void wall; thus, volume ionization plays a significant role. As the rate of electron generation due to volume ionization is much lower than the surface emission, there is a considerable inception delay time before the occurrence of the first PD. Volume ionization might occur due to the irradiation of energetic photons (mechanism VI) or field detachment of electrons from negative ions (mechanism VII) [34]. The electron generation rate due to volume ionization (\dot{N}_{vol}) is dominated by irradiation of energetic photons and can be calculated as [34, 70]:

$$\dot{N}_{vol} = C_{rad} \phi_{rad} \left(\frac{\rho}{p}\right)_0 p V_{eff} \quad (3.9)$$

where C_{rad} is a parameter for modeling the interaction between gas molecules and radiation, ϕ_{rad} is the quantum flux density of the radiation (at atmospheric pressure: $C_{rad} \phi_{rad} = 2 \times 10^6 \text{ kg}^{-1} \text{ s}^{-1}$), and $(\rho/p)_0 = 10^{-5} \text{ kg} \cdot \text{m}^{-3} \cdot \text{Pa}^{-1}$ is the pressure reduced density of the gas. The term V_{eff} stands for the void volume. For an ellipsoidal void, it equals $4\pi abc/3$ where a , b , and c are the axes of the ellipsoidal void. In [34], another term called the Legler function, $(1 - \eta/\alpha)$, multiplies the right-hand side of (7); it

considers the probability that the electron can lead to an electron avalanche. The parameters η and α stand for the gas attachment coefficient and the gas ionization coefficient, respectively. In the PD phenomenon, usually $\eta \ll \alpha$, which makes the Legler function close to unity. However, as the whole electron generation rate will later be employed to find the probability of PD occurrence, it would be unnecessary to involve the Legler function to evaluate the probability of avalanche ignition.

3.3.2 Experimental-based Representation

As the theoretical-based formulations of electron generation processes discussed in Section ?? require some physical parameters that are not widely available, a somewhat simplified model has been introduced in [64, 65, 67, 69, 71] based on adjustment of the experimental results. By neglecting the contribution of volume ionization, the electron generation rate ($\dot{N}_{tot}(t)$) was modeled as [65]:

$$\dot{N}_{tot}(t) = N_{es} \exp\left(\left|\frac{E_{cav}(t)}{E_{inc}}\right|\right) \quad (3.10)$$

where N_{es} is a constant, $E_{cav}(t)$ is the electric field intensity inside the void, and E_{inc} is the inception field for discharge. A more sophisticated model taking both electron generation processes into account was proposed in [64, 67, 69, 71]:

$$\dot{N}_{tot}(t) = \dot{N}_{surf}(t) + N_{vol} \quad (3.11)$$

where N_{vol} is a constant representing the contribution of volume ionization. The electron generation rate due to surface emission $\dot{N}_{surf}(t)$ is assumed to be proportional to the PD charge magnitude of previous events since they are the resources of trapped electrons at the

void surface. Thus, $N_{surf}(t)$ can be calculated by [64]

$$\dot{N}_{surf}(t) = N_{PD} \exp\left(\left|\frac{E_{cav}(t)}{E_{inc}}\right|\right) \exp\left(-\frac{t - t_{PD}}{\tau_{decay}}\right) \quad (3.12)$$

where the first exponential term considers the effect of the electric field, and the second one represents the decay of PD charges by time after its occurrence at t_{PD} . The PD charge magnitude is modeled as:

$$N_{PD} = N_{es0} \left| \frac{E_{cav}(t_{PD})}{E_{inc}} \right| \quad (3.13)$$

where N_{es0} is assumed to be the incipient number of electrons at the time that electric field inside the void reaches the inception field E_{inc} . The constants N_{vol} , N_{es0} , and τ_{decay} are determined in a way to have an acceptable level of agreement with experimental results.

3.3.3 Probability of PD occurrence

The last step to ensure the initial electron availability is to take the stochastic property into account. Firstly, at each time step, the probability of free electron existence, (P), is estimated: [60, 65]:

$$P(t) = 1 - \int_{t_{PD}}^{t_{PD}+t} \dot{N}_{tot}(\tilde{t}) d\tilde{t} \quad (3.14)$$

Thereafter, the probability is compared to a random number R between zero and unity. If $P > R$, the electron availability at the certain time step is confirmed; otherwise, a time step is added to the statistical time lag before PD occurrence.

3.4 PD Transient State

3.4.1 Conductive State of PD

Once the above PD prerequisites are met, the occurrence of PD changes the state of the cavity from non-conducting to conducting. In the FEA model, the discharge is modeled as an increase in the conductivity of the void from an initial value ($\sigma_{cav,0}$) to a maximum level ($\sigma_{cav,max}$). The increase in the void conductivity causes a voltage drop across the void as well as a field reduction inside the void. The discharge continues until a certain value of the electric field at which the ionization cannot go any further. After the extinction of PD, the conductivity of the void is returned to its initial value. However, the charges deposited on the void wall can help to accelerate the happening of the next PD event. To validly obtain the physical and apparent charge magnitude, an appropriate time-varying conductivity which has low value before PD occurrence and rises to a higher value during PD occurrence should be defined. This is crucial for the estimation of current density over cavity wall or electrode surface since current density is the parameter used in calculation of the true and apparent charge magnitudes. $\sigma_{cav,max}$ is defined as follows [72]:

$$\sigma_{cav,max} = \frac{\alpha e^2 N_e \lambda_e}{m_e c_e} \quad (3.15)$$

Where:

$$N_e = \frac{q_{max}}{4/3\pi e r^3} \quad (3.16)$$

Where c_e is the thermal velocity, and λ_e is the electron mean free path. α is a coefficient related to the electron energy distribution and the mean free path. r is the cavity radius

while e and m_e are the elementary charge and mass, respectively. q_{max} is the maximum physical charge amount. It can be obtained for a spherical cavity as [52]:

$$\frac{q_{max}}{q_{min}} \cong 2\nu \quad (3.17)$$

where:

$$q_{min} \cong \frac{\pi\epsilon_0}{4}(2\epsilon_r + 1)\left(\frac{E}{p}\right)_{cr}pl^2\left[1 - \gamma + \frac{B}{(pl)^n}\right] \quad (3.18)$$

ν is the overvoltage ratio (the applied voltage to the inception voltage). γ is the ratio of streamer field to a critical field which is around 0.2 for air when applying a positive polarity voltage.

3.4.2 Charge Calculation

With the aid of FEA, the electrical parameters, such as field displacement and current density over different parts of the system, can be accessed. This helps to dynamically examine the changes in the electrical characteristics of PD phenomena before, during, and after its occurrence. Thanks to the privilege of FEA, the magnitude of true and apparent charges related to each PD event can be obtained through the time integration of the current flowing through the void surface and electrode, respectively during a PD event given by

$$q_{true} = \int_{t_{inc}}^{t_{ext}} \int_{S_{cav}} \vec{J}(t) \cdot d\vec{S} dt \quad (3.19)$$

$$q_{app} = \int_{t_{inc}}^{t_{ext}} \int_{S_{Electr}} \vec{J}(t) \cdot d\vec{S} dt \quad (3.20)$$

In the above equations, $\vec{J}(t)$ is the current density over either the void surface in 3.19 or the electrode in 3.20. For the calculation of true apparent charge, the current over the upper half-area of the void is integrated between the inception and extinction time. A similar procedure is repeated for the apparent charge; however, in this case, the current over the ground electrode is used for derivation of charge magnitude.

3.5 Charge Decay

The produced charges during a PD might decay through various ways including ion drift, charge neutralization, and surface conduction which usually has the main effect. Surface conductivity, σ_s , is strongly dependent on temperature and the electric field intensity across the cavity [64]. For a constant temperature, it can be defined as:

$$\sigma_s(t) = \sigma_{s0} \exp(\alpha |E_{cav}(t)|) \quad (3.21)$$

Where σ_{s0} is the initial surface conductivity ($\simeq 10^{-18} Sm^{-1}$), and α is the surface conductivity coefficient ($\simeq 10 mmkV^{-1}$).

As mentioned earlier, the amount of charges accumulated on the void surface varies over time; during electron avalanche, the number of electrons increases, and these generated electrons will decay between PD events. In section 3.3, it was discussed how to consider the impact of surface charge decay on the electron generation rate. However, in the FEA model, the contribution of surface charge decay should also be involved in the dynamic modeling of PD. The trapped charges can hop into deeper traps, which makes it harder to detrap electrons for PD ignition, yet they take part in the potential difference across the void [64]. Electrons may also decay through diffusing into the depth of the insulating material [52], which can

affect the charge density on the void surface. To model the decay rate, surface conductivity can be adjusted. In [65], a charge-dependent model is proposed for surface conductivity. The surface conductivity is assigned an initial value ($\sigma_{surf,L}$). Once the electric charge on the void surface exceeds a critical amount (q_{cr}), the surface conductivity will be enhanced to a higher value ($\sigma_{surf,H}$). If the charge magnitude falls below q_{cr} again, the surface conductivity will be re-assigned its initial value ($\sigma_{surf,L}$). In [64], a field-dependent surface conductivity formula was introduced. Surface conductivity ($\sigma_s(t)$) increases from its initial value (σ_{s0}) to a higher value, which is given by a field-dependent formulation [64]:

$$\sigma_s(t) = \sigma_{s0} \exp(\alpha |E_{cav}(t)|) \quad (3.22)$$

where α is the stress coefficient. In [64], a maximum value for σ_s estimated through the experimental data and given by Eq. 3.23 was used to avoid convergence problems.

$$\sigma_{s,max} = \gamma \exp(\beta |E_{app}(t)|) \quad (3.23)$$

where γ and β were experimentally determined. However, a prerequisite for using the above formula is to ensure the existence of free surface charges at the void surface. Charges at the void surface are grouped into two types: the first group consists of the trapped charges at the void surface, which was discussed before, and the other type includes free charges in the same area. The free charges can be approximated by the integration of field displacement over the upper or lower void surface (S_{void}) as:

$$q_{free}(t) = \int_{S_{void}} D(t) \cdot dS \quad (3.24)$$

Then, the magnitude of the electric field due to this second group of charges ($E_{s,free}(t)$) can

be calculated by:

$$E_{s,free}(t) = \left| \frac{q_{free}(t)}{q_{PD,total}(t)} E_{int}(t) \right| \quad (3.25)$$

where $q_{PD,total}$ is the total amount of true charge originating from the PD events that happened so far. As seen in Figure 3.1, the electric field inside the void ($E_{cav}(t)$) consists of two components: (1) the electric field due to the applied voltage ($fE_{app}(t)$) and (2) the electric field due to the surface charges ($E_{int}(t)$). Therefore, the electric field due to surface charges can be obtained as follows:

$$E_{int}(t) = E_{cav}(t) - fE_{app}(t) \quad (3.26)$$

where f is the enhancement factor, which takes into account the impact of void existence on the increase in the electric field magnitude at the location of the void. In other words, $fE_{app}(t)$ is the electric field at the location of the void in the absence of surface charges. f can be obtained from the following equation [52]:

$$f = \frac{K\epsilon_r}{1 + (K - 1)\epsilon_r} \quad (3.27)$$

where K is a geometrical parameter given by [52]:

$$K = \begin{cases} \sim 1 & a/b \ll 1 \\ 3 & a/b = 1 \\ \sim \frac{4a}{b} & 1 < a/b < 10 \end{cases}$$

where a and b are the ellipsoid axes parallel and perpendicular, respectively, to the background field.

3.6 Algorithm

As disclosed earlier, the electric field intensity plays a major role in different sections of PD modeling. Therefore, an accurate estimation of the electric field distribution is crucial to the whole process. In this regard, the current study employs FEA to utilize the capabilities of the finite-element method to accurately estimate the electric field distribution within the air filled-cavity, dielectric system.

In this work, COMSOL Multiphysics is used to implement FEA. MATLAB is also used along with COMSOL to model the other parts of the algorithm such as checking PD occurrence prerequisites and calculating the true and apparent charge magnitudes.

To calculate the true and apparent charge magnitudes, the algorithm uses one of the outputs of COMSOL, which is the current density flowing through the cavity wall and ground electrode. Then, by integrating the current density over time, starting from inception and going to extinction, the charge magnitudes are obtained.

When a PD occurs, it is accompanied by an enhancement in cavity conductivity that further causes a decline in electric field across the cavity. To model PD transient state, when the two PD prerequisites are met, the void conductivity rises from the initial value (usually zero) to a higher value ($\sigma_{cav,max}$).

Furthermore, the charges accumulated on the cavity wall do not last infinitely; a main decay process occurs by the charges moving from shallow traps to deeper ones which causes conduction along cavity surface [64]. The decay rate is a function of the amount of charge accumulated over the cavity wall. The decay process can be modeled as follows: there is a critical value for the amount of deposited charge (q_{cr}); if the magnitude of physical charge on the surface goes above this value, the conductivity of cavity wall increases from $\sigma_{surf,L}$ to $\sigma_{surf,H}$ [68]. This transition reduces the accumulation of surface charges. The surface

conductivity remains at the high level until the amount of charges falls below the critical level. As seen, the charge magnitude is a required quantity in this model. In the FEA approach, the charge magnitude can be easily obtained by integrating field displacement over the surface area.

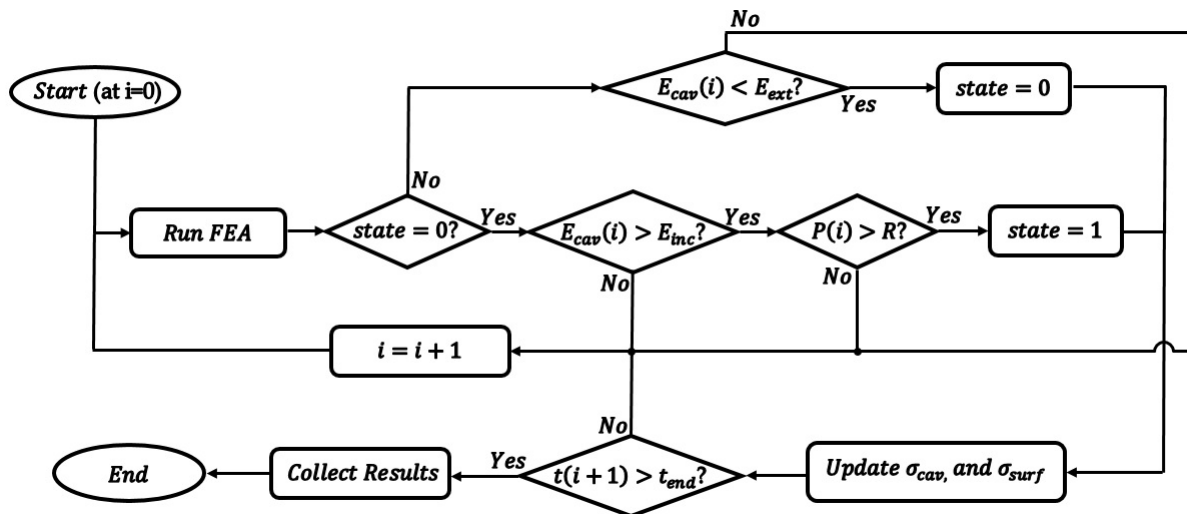


Figure 3.2: PD modeling flowchart.

The PD modeling process is showed utterly in Fig. 3.2. Starting from the beginning of the period, the electric field distribution is obtained by FEA model to evaluate the PD occurrence requirements (i.e. streamer inception criterion and the availability of initial free electron). The process adds a time step to the time until reaching a moment that both PD conditions are met or the process reaches the end of time period. For the times that the occurrence of PD is confirmed, the conductivities of cavity and its surface is enhanced as explained earlier in this chapter. In the next time steps, the PD extinction is looked for after running FEA. As demonstrated in Fig. 3.2, a state variable is used to model the transitions between no-PD (state=0), and during-PD (state=1) periods. The time steps referred to during this algorithm may vary according to the state. As the changes during PD are in order of nano-seconds, the time step during PD (Δt_L) is much smaller than the time step during no-PD (Δt_H) period.

3.7 Summary

In the first section, the streamer inception criterion was examined in detail which ensures the first condition for PD occurrence. Then, the initial electron generated condition was formulated using various models. The Niemeyer representation of the initial electron generation consists of two main resources: (1) surface emission through detrapping of electrons from the pores of the cavity wall. These electrons are trapped after the accumulation of PD charges. (2) volume ionization which occurs after irradiation of energetic photons to the atoms/-molecules. This process is dominant only when the surface emitted electrons are unavailable (such as the case of the first PD event where no prior discharges have occurred). Aside from Niemeyer representation, Forssen and Illias also proposed simplified versions of electron generation rate based on experimental results. Forssen neglected the volume ionization share of total electron generation and expressed total electron generation as an exponential function of electric field magnitude. On the other hand, Illias used similar representation; however, in his model, he considered the volume ionization as a constant number in the total electron generation rate. After that, the charge decay process was formulated as a function electric field to represent the memory effect. Finally, an algorithm using all the aforementioned processes was developed.

In the next chapter, the numerical studies for two case studies on which the proposed algorithm was applied will be presented.

Chapter 4

Numerical Results

4.1 Case Studies

4.1.1 Case 1:

The geometry considered for modeling and simulations is the same as that used in [69] as shown in Fig. 4.1. It is a cylindrical block of epoxy resin ($\epsilon_r = 5.2$) with a spherical cavity

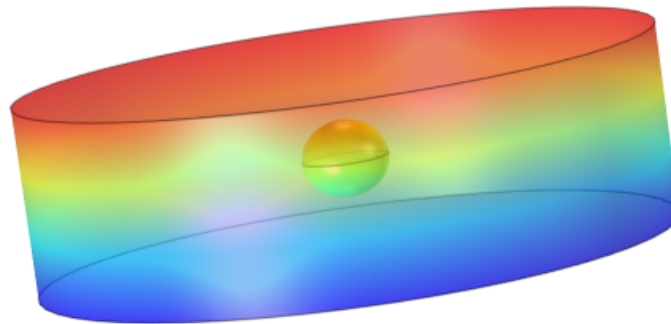


Figure 4.1: 3D representation of 1st case study.

inside it. The geometrical parameters of the void-dielectric set are brought in Table 4.1. Also, the properties of the applied voltage are summarized in Table 4.2.

Due to the axial symmetry of the configuration, a 2D axisymmetric model is developed in COMSOL Multiphysics (shown in Fig. 4.2). To validate our FEA model developed in COM-

Table 4.1: Geometrical Parameters of 1st Case

Parameter	Value
Dielectric Thickness	3 mm
Dielectric Radius	5 mm
Cavity Diameter	1.2 mm
Cavity Surface Thickness	0.05 mm

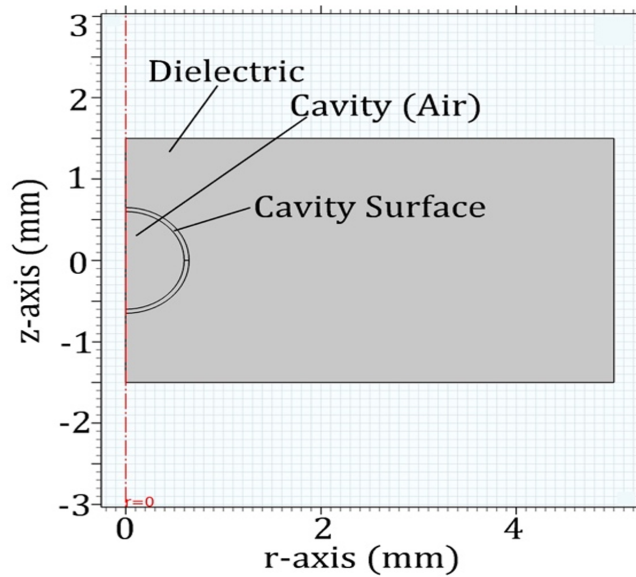


Figure 4.2: 2D representation of 1st case study.

SOL Multiphysics, first, the simulation results reported in [27] under an $18kV$ and $50Hz$ sinusoidal voltage were reproduced. Then, the applied voltage was changed to a square wave with the specifications listed in Table 4.2. By assuming the duty cycle to be 50%, U_{max} is calculated in a way that the RMS value of the square wave is equal to that of the sinusoidal voltage considered in [69]. The details and representation of the mesh are shown in Table 4.3 and Fig. 4.3, respectively.

Finally, the parameters related to the dielectric, electron generation rate, decay rate along with algorithmic parameters such time steps are all brought in Table 4.4.

Table 4.2: Square Wave Voltage Parameters for 1st Case

Parameter	Value
U_{max}	18 <i>kV</i>
f	3 <i>kHz</i>
Rise Time	1 μs
Duty Cycle	50%

Table 4.3: Mesh Properties of 1st Case

Quantity	Value
Maximum element size	$2.65 \times 10^{-4} m$
Minimum element size	$1.5 \times 10^{-6} m$
Maximum element growth rate	1.3
Curvature factor	0.3
Resolution of narrow regions	1

Table 4.4: PD Parameters for 1st Case

Symbol	Value
ϵ_r	4.4
σ_0	$10^{-18} S/m$
E_{cr}	$2.42 \times 10^6 V/m$
N_{surf0}	3000
N_{vol}	2
p	1 <i>atm</i>
τ_{decay}	0.002 <i>s</i>
T	300 <i>K</i>
Δt_H	$1/(1000f)$
Δt_L	$1/(1000 \times 500f)$
$\sigma_{cav,max}$	0.001 <i>S/m</i>
$\sigma_{surf,L}$	$10^{-15} S/m$
$\sigma_{surf,H}$	$2 \times 10^{-11} S/m$
E_{inc}	3.1 <i>kV/mm</i>
E_{ext}	0.1 <i>kV/mm</i>

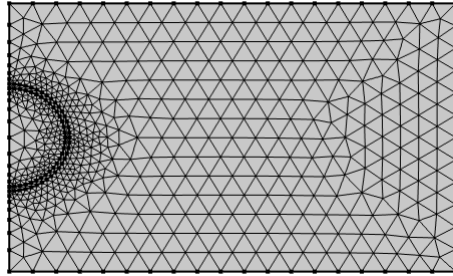


Figure 4.3: Mesh pattern of 1st case study.

4.1.2 Case 2:

The case study consists of a sphere-sphere electrode system that provides a weakly non-uniform electric field. It consists of two spherical electrodes; one is the high-voltage electrode while the other is grounded. The two spheres are situated within a cylindrical block of silicone gel ($\epsilon_r = 2.7$ at NTP) with a spherical air-filled cavity inside shown in Fig. 4.4. The geometric parameters of the void-dielectric set are shown in Table 4.5. For FEA, the

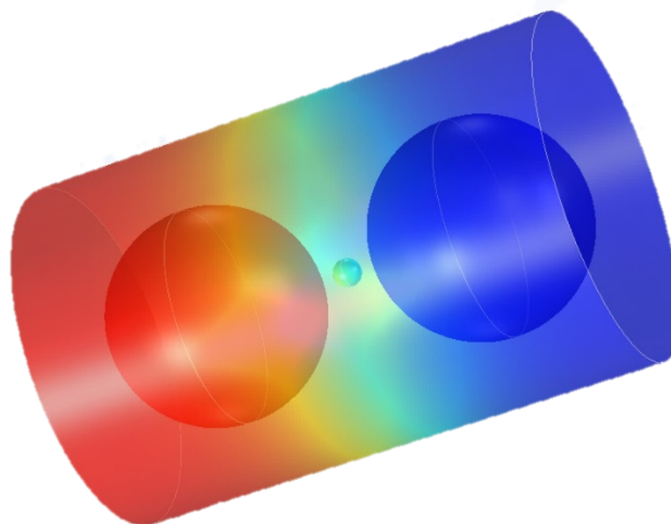


Figure 4.4: 3D representation of 2nd case study.

2D-axisymmetrical representation of the configuration is used (see Fig. 4.5). Moreover, the properties of the square wave voltage which is applied to the insulation system are listed in

Table 4.5: Geometrical Parameters of 2nd Case

Parameter	Value
Electrode Radius	5 mm
Distance between Electrodes	3 mm
Dielectric Radius	8 mm
Dielectric Height	25 mm
Cavity Diameter	1 mm
Cavity Surface Thickness	0.05 mm

Table 4.6: Square Wave Voltage Parameters for 2nd Case

Parameter	Value
U_{max}	11 kV
f	20 kHz
Rise Time	100 ns
Duty Cycle	50%

Table 4.6. The details and representation of the mesh are shown in Table 4.7 and Fig. 4.6,

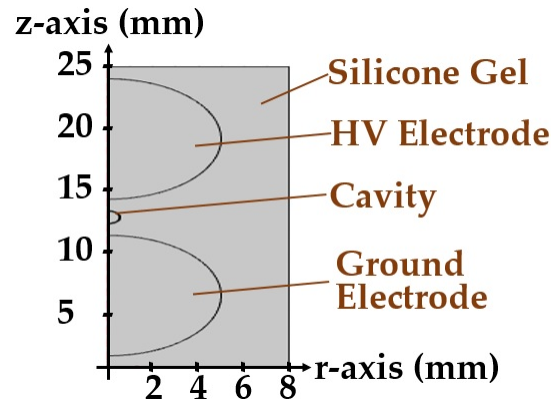


Figure 4.5: 2D representation of 2nd case study.

respectively. The parameters related to electron generation rate, time-stepping, and charge decay are listed in Table 4.8.

Table 4.7: Mesh Properties of 2nd Case

Quantity	Value
Maximum element size	$5 \times 10^{-4} m$
Minimum element size	$1.88 \times 10^{-6} m$
Maximum element growth rate	1.2
Curvature factor	0.25
Resolution of narrow regions	1

Table 4.8: PD Parameters for 2nd Case

Symbol	Value
ϵ_r	2.8
σ_0	$10^{-13} S/m$
E_{cr}	$2.42 \times 10^6 V/m$
K_{rad}	$2 \times 10^6 kg-1s^{-1}$
$(\rho/p)_0$	$10^{-5} kgm^{-3}Pa^{-1}$
p	1 atm
τ_{decay}	0.15/f
ϕ	1.3 eV
ν_0	$10^{14} s^{-1}$
T	300 K
Δt_L	1/(1000f)
Δt_H	1 ns
$\sigma_{cav,max}$	0.0004 S/m
$\sigma_{surf,L}$	$2 \times 10^{-13} S/m$
$\sigma_{surf,H}$	$10^{-11} S/m$
E_{inc}	3.1 kV/mm
E_{ext}	0.1 kV/mm

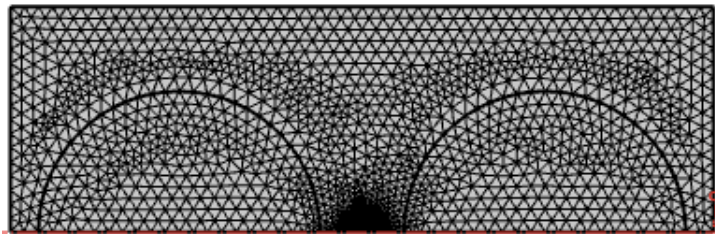


Figure 4.6: Mesh pattern of 2nd case study.

4.2 Electric Field Distribution

Fig. 4.7 and Fig. 4.8 shows the electric field distribution of the cavity-dielectric system in the 1st case before and right after the moment PD takes place. As expected, the intensity

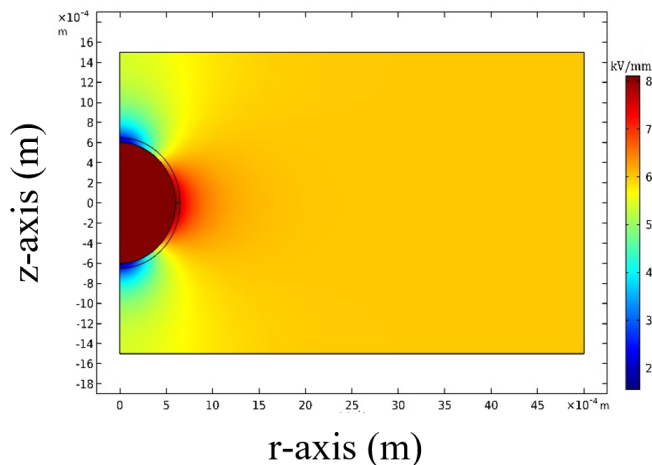


Figure 4.7: The whole system electric field distribution before PD occurrence.

of electric field across the cavity is higher than dielectric material due to the lower (by a factor of $\frac{3\epsilon}{2\epsilon_r+1}$ [34]) dielectric constant in air rather than insulating medium. As discussed earlier, charges deposit on the cavity wall after occurrence of PD. This adds up another field component beside the main component imposed by the applied voltage. However, this component opposes the main component. During the PD, the electric field inside the cavity goes down to almost zero bringing it even lower than the material in its surrounding. This is a typical behavior one anticipates from a discharge regardless of the type of applied voltage.

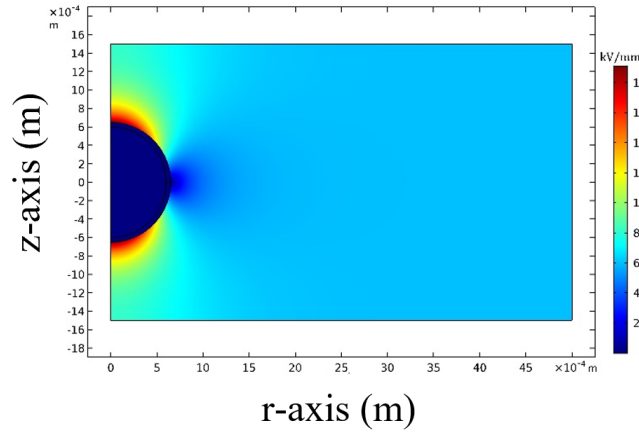


Figure 4.8: The whole system electric field distribution after PD occurrence.

The radial and axial electric field distributions are shown in Figs. 4.9 and 4.10 right before and right after the 1st discharge. The results validates the previous discussion on the electric field variations. Furthermore, it is demonstrated that by increasing the cavity size, the field intensity in z-direction goes down and the radial component loses a portion of its uniformity.

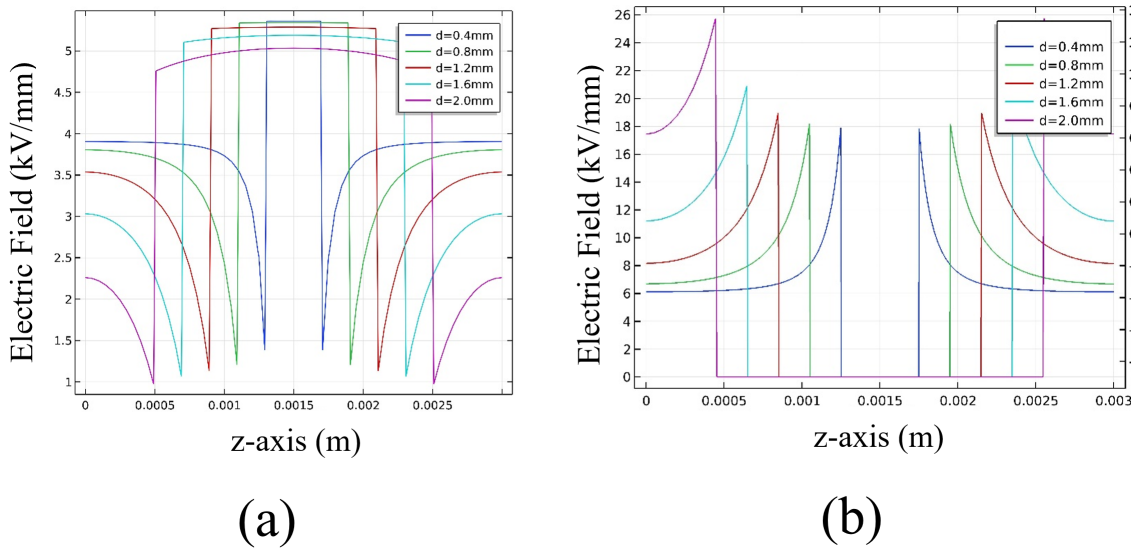


Figure 4.9: Axial electric field distribution after PD occurrence.

For the 2nd case, Fig. 4.11 indicates the field distribution before and after the discharge.

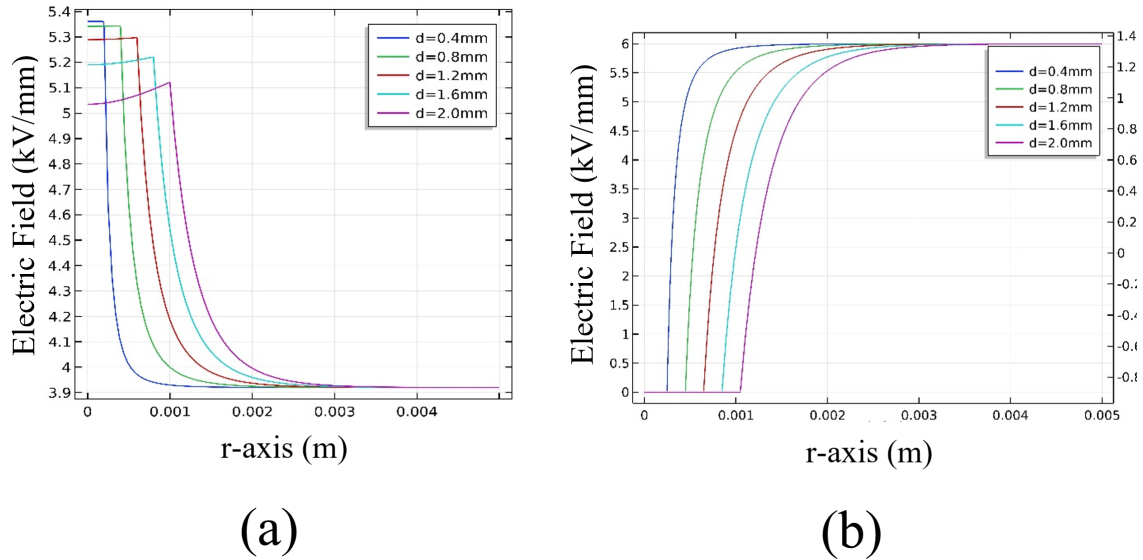


Figure 4.10: Radial electric field distribution after PD occurrence.

Same as previous case, the field intensity across the void is higher than other parts. As the voltage keeps increasing, the cavity electric field goes up until a moment at which the cavity cannot tolerate the stress. At this point, once the initial electron is provided, the electron accelerates, collides with other atoms, and ignites the electron avalanche. Subsequently, the conductivity of cavity enhances, leading to a reduction of electric field as well as a voltage drop across the cavity. This keeps going until the electric field falls below the extinction field.

4.3 PD Charge Magnitude

Fig. 4.12 shows the phase-resolved PD (PRPD) pattern for 1st case study. Also a summary of PD charge results are demonstrated in Table 4.9. In this table, the PD intensity is characterized using two charge magnitudes, one the charge accumulated over the cavity wall (true charge), and the other one is the deposited charge on the electrode (apparent charge).

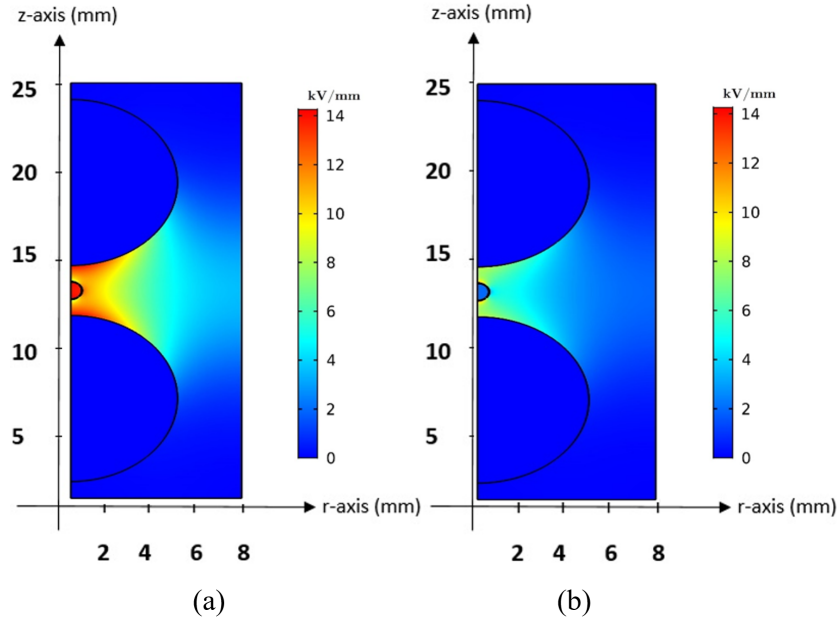


Figure 4.11: Electric field distribution in 2nd case.

Table 4.9: PD Results for 1st Case

Quantity	Value
Average number of PDs per cycle	2.87
Mean true charge magnitude	745.09 pC
Mean apparent charge magnitude	204.29 pC
Maximum true charge magnitude	1985.6 pC

A summary of the results for 2nd case study is reported in Table 4.10. Also, Fig. 4.13 shows the phase-resolved PD (PRPD) pattern in this case. What these results demonstrate agrees with what had been observed in experiments [47]. Two discharges take place per cycle; one on the side where voltage is rising, and the other one on the side that voltage is dropping. While the charge magnitudes almost the same for these two discharges, Fig. 4.13 implies that on the falling flank, it takes more time for the discharge to occur (higher time lag). The reason lies in the higher time delay at the falling flank to provide the initial electron owing to the charge decay.

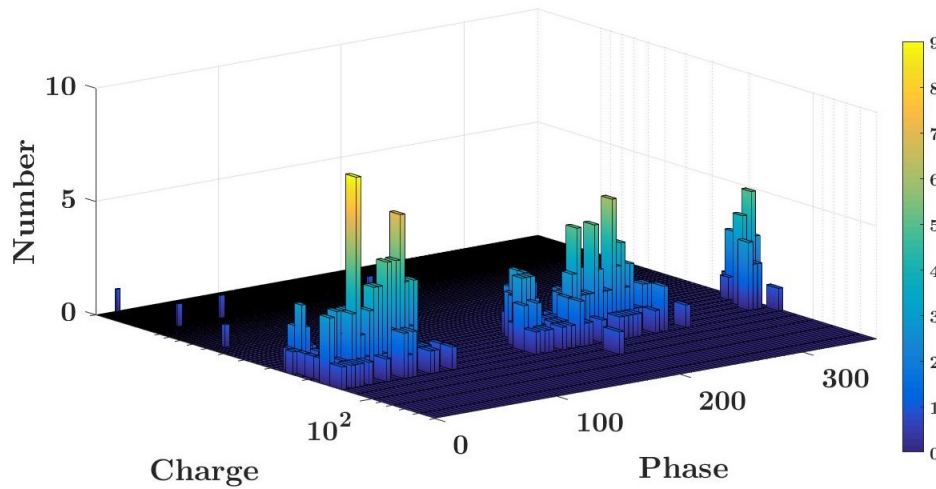


Figure 4.12: PRPD pattern for 1st case study.

Table 4.10: PD Results for 2nd Case

Quantity	Value
Average number of PDs per cycle	1.9866
Mean true charge magnitude	0.420 μC
Mean apparent charge magnitude	14.88 μC
Maximum true charge magnitude	2.46 μC

4.4 Impact of Cavity Characteristics

4.4.1 Cavity Diameter

Fig. 4.14 demonstrates the impact of void size on the field intensity at the center of the cavity for the 1st case. Same as the case of sine wave, the field intensity across the void does not sharply decrease by augmenting the cavity diameter, specifically for smaller voids. Fig. 4.15 shows the difference in inception voltage among the two voltage types. In both cases, the voltage peak is 18 kV .

The figure implies that the 3 kHz square wave has higher inception voltage compared to the sine wave. However, the results have indicated that at higher frequencies of square wave, it

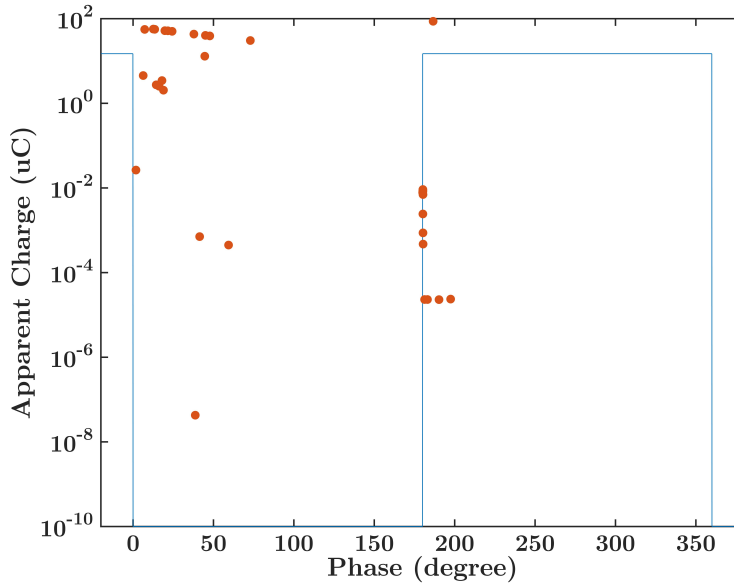


Figure 4.13: PRPD pattern for 2nd case study.

has an inception field much closer to that of sine wave. For the frequency of 30 kHz , the inception voltage-diameter relationship is almost the same as the 50 Hz sine wave, shown in Fig. 4.15. Therefore, one can conclude that as the frequency goes higher, the discharges rate enhances while PDs also take place at lower voltages. Fig. 4.16 shows the relationship between the cavity diameter and inception electric field. As implied by the figure, the electric field at which PD ignites has a direct relationship with cavity size. To justify this observation, one should consider that by the growth of diameter, a more uniform field will be at the center void, making it harder to bridge the cavity [64].

During the manufacturing process, the formation of voids is unavoidable, and it is vital to comprehend the impact of void size to be able to efficiently benefit from techniques for the reduction in void number and size. Figure 9a shows the variation of apparent and true charges to changes in the void radius. The results imply that as the size of the void increases, the intensity of PD is escalated. This can be justified by mentioning that for larger voids, the void surface is larger. Moreover, the larger air gap needs higher electric field intensity to

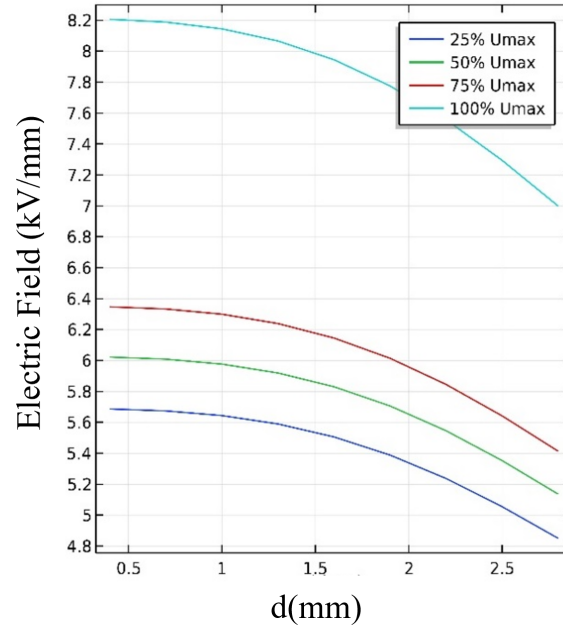


Figure 4.14: Effect of diameter on electric field magnitude in 1st case.

breakdown; therefore, it may be expected that those PDs occurring at higher electric fields have higher intensities due to Ohm's law ($J = \sigma E$).

4.4.2 Cavity Location

In order to assess the effect of cavity location on PD inception, the center of cavity moved along both r-axis and z-axis. Fig. 4.18 and 4.19 show the results after the variation of r- and z-axis component, respectively. Moving the cavity along r-axis will not substantially change the inception voltage unless it makes the cavity too close to the sides of dielectric. On the other hand, when the cavity moves along the z-axis, the inception voltage is significantly decreased in each direction.

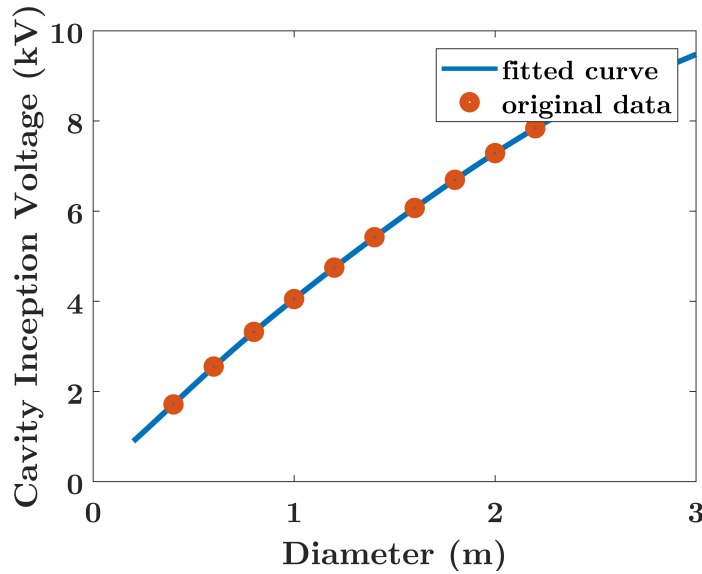


Figure 4.15: Impact of voltage shape.

4.4.3 Cavity Shape

To address the impact of cavity shape, the shape of the cavity is changed from an oblate spheroid (similar to a flat cavity) to a prolate spheroid (similar to a bar-shaped cavity), while keeping the volume of cavity constant. Fig. 4.20 demonstrates that when the shape of the cavity changes from a sphere to a spheroid (either prolate or oblate), the inception voltage goes up. It means that the spherical cavity has a minimum tolerance against PD occurrence. It is crystal clear that there are arbitrary shapes for voids which are hardly possible to be defined mathematically. However, in order to classify voids and evaluate the impacts of each class on the occurrence of PD, different shapes for voids should be considered. In this regard, the original spherical shape examined is generalized to a spheroidal shape, which can differ from an oblate to a prolate spheroid. An oblate void can be classified in the group of flat voids. On the other hand, the prolate shape can be assigned to the class of bar-shaped voids. It is assumed that during the changes in the void shape, its volume is kept constant.

Fig. 4.21 compares the true charge magnitudes of PD as a function of the vertical radius

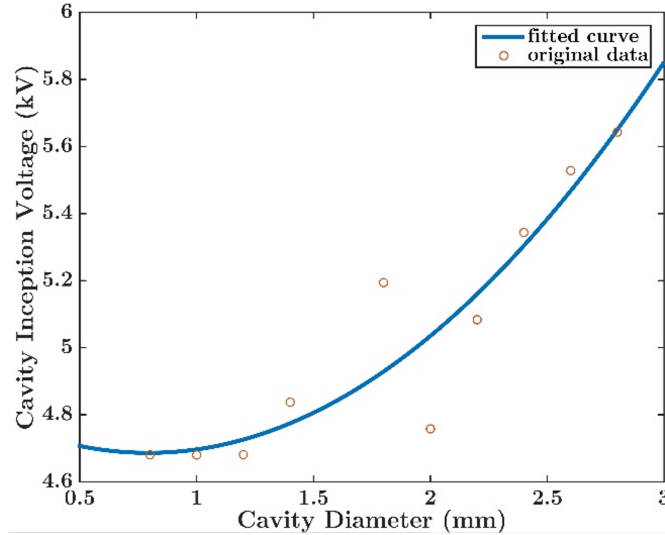


Figure 4.16: Impact of cavity diameter on PD charge magnitude.

(r_z). The results show that the intensity of PD is escalated by having a prolate void shape rather than an oblate one. The latter conclusion can be reasoned through the longer air-gap along the electric field direction (z -direction). Hence, the long gap requires a higher electric field to break, and it is anticipated that at higher field intensities, the current density and, subsequently, the charge magnitudes have higher amounts.

4.5 Impact of Applied Voltage Parameters

As seen in Figure 4.22, and 4.23, the destructive impact of frequency and rise-time on PD charge magnitude is clear. However, among these two factors, frequency is more detrimental at its high values. It should also be noted that the number of PDs per cycle may decrease by a frequency enhancement, but the severity of PDs is escalated. The dependency of PD inception on rise-time is demonstrated in Fig. 4.23. At first glance, it can be inferred that as the rise-time increases, the PD happens at a lower electric field magnitude. However, it does not necessarily state that PD happens quicker, since the increase in the rise-time, rises the

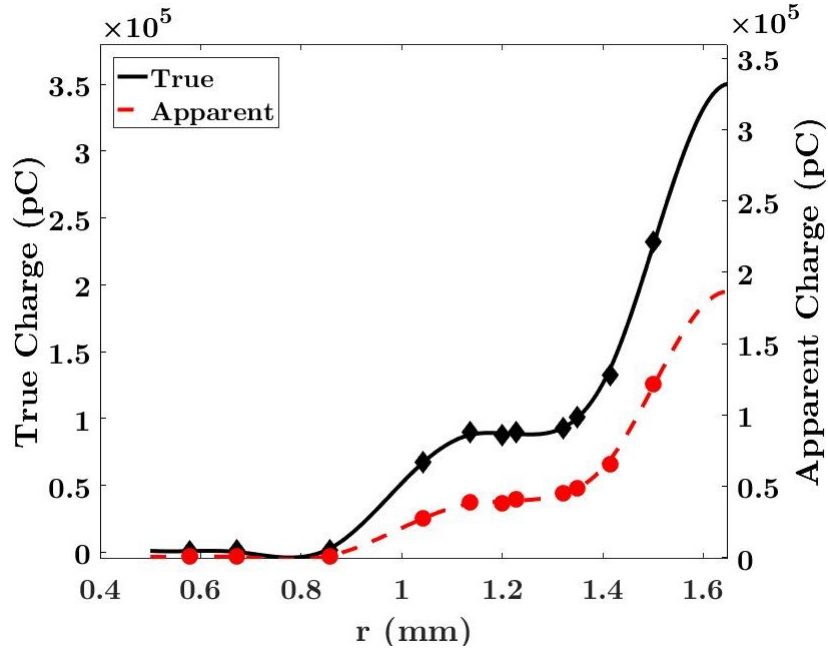


Figure 4.17: Impact of cavity diameter on PD charge magnitude.

PD inception time itself. The impact of PD charge magnitude is shown in Fig. 4.24. The figure shows that at from a certain rise time value, the decrease in in this quantity can lead to an exponential increase in the PD charge magnitude. Therefore, it is great significance to investigate new materials or techniques that can enhance the resistivity of insulation against ultra-fast rise square waves.

4.6 Impact of Pressure

Nowadays, electrification is penetrating various technologies such as aircraft, where one of the lesser known parameters in the path toward electrification is pressure. During flights, an aircraft can undergo low-pressure conditions as low as $4psi$. Therefore, it is of great significance to delve into a reliability analysis of the insulation system under these severe conditions. Different mechanisms within the PD-related processes depend on pressure.

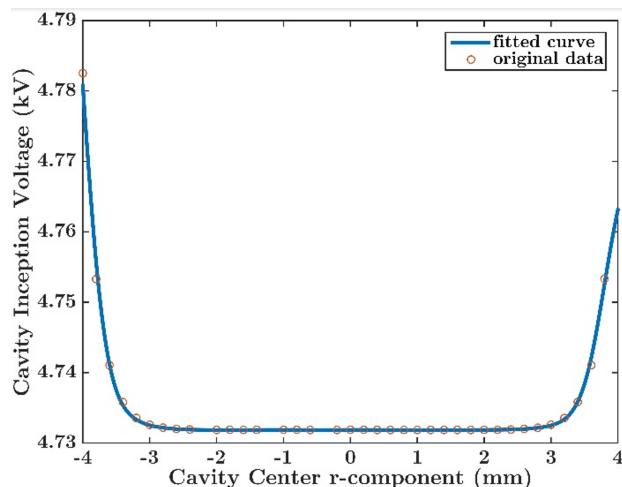


Figure 4.18: PD inception voltage as a function of location in r-axis.

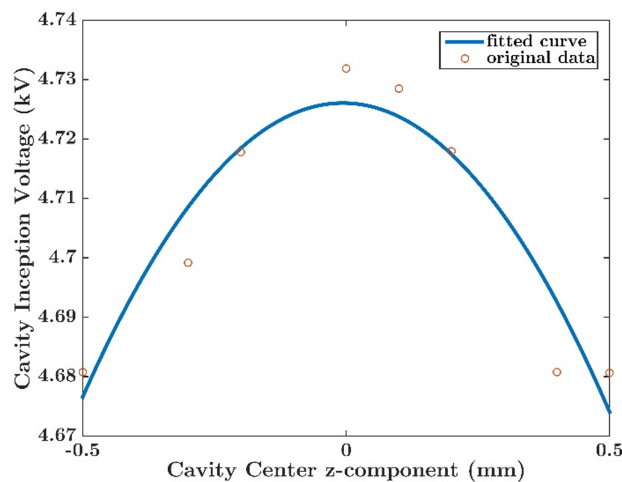


Figure 4.19: PD inception voltage as a function of location in z-axis.

The inception electric field (E_{inc}) has an inverse relationship with pressure, meaning that as the pressure decreases, E_{inc} goes higher. However, one should not quickly infer that higher values lead to more resistance against PD threats; this is due to the higher magnitude of induced charge that the corresponding PD might have. Pressure also has an impact on the magnitude of the extinction electric field (E_{ext}). It was alleged in [73] that E_{ext} has a direct relationship with pressure. The latter conveys the fact that at lower pressures, the electric field at which PD is quenched becomes lower than the expected value.

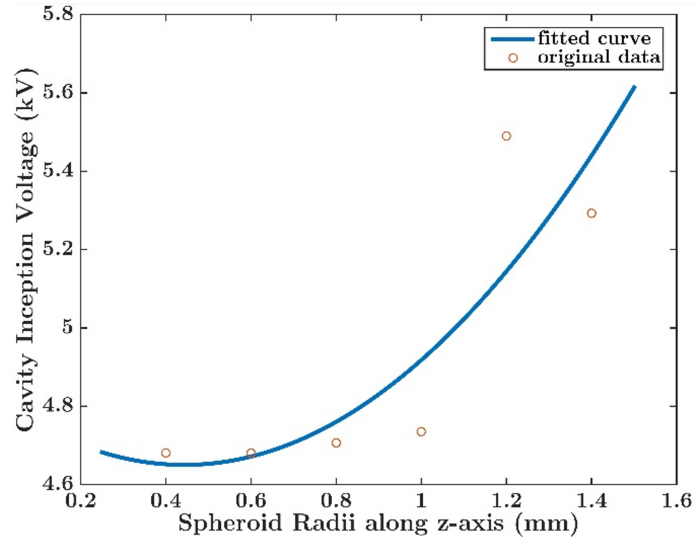


Figure 4.20: Impact of cavity shape on inception voltage.

Fig. 4.25 demonstrates that E_{inc} and E_{ext} have opposite trends with pressure variation. E_{inc} is a decreasing function of pressure, while E_{ext} is an increasing function. As will be shown later, these two trends play a significant role in PD characteristics such as PD inception and extinction times, intensity, etc.

The rest of this section focuses on the variations of several PD characteristics with pressure. Simulations are performed for 15 pressure values which are shown in red points in Figs. 4.26-4.28. Then, the trends of the variations denoted as fitted curve in Fig. 4.26-4.28 are derived over a continuous range of pressures using smoothing spline interpolation technique.

Fig. 4.26 reflects the impact of pressure on the inception time of PDs. Higher inception time values at lower pressures can be explained by the fact that as the pressure decreases, E_{inc} goes up. As E_{inc} increases, the PD demands more time to catch a higher electric field value. A quick conclusion might be that the later PD occurs, the longer the insulation material can withstand degradation; however, as will be discussed next, a bit later discharges impose more intense ones.

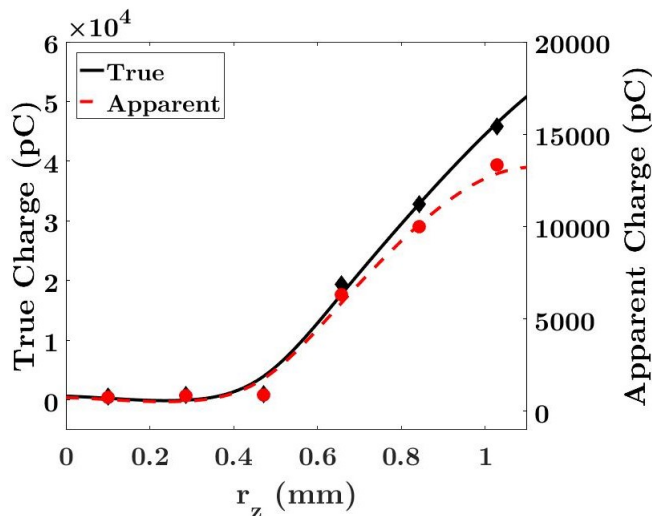


Figure 4.21: The impact of cavity shape on PD charge magnitude

Similarly, the extinction time trend can be justified; at lower pressures, the linear function of the extinction field, with respect to pressure, trends downward as well. To quench a discharge at lower field magnitudes, more time in the high-conductivity period is needed to reduce the electric field intensity. Thus, like inception time, extinction time is also higher for lower pressures. Since both inception and extinction times increase with pressure reduction, what happens to the duration of PD at lower pressures? Fig. 4.27 indicates that the duration of discharges at lower pressures are higher than NTP conditions. Thus, it can be inferred that, under low-pressure conditions, the prolongation of PDs due to later extinction times is much higher than the shortening of PDs due to later inception times. This difference tends to decline as the pressure goes up.

Fig. 4.28 shows variations of PD true charge magnitude as a function of pressure. The results affirm that as the pressure is reduced, the PD magnitude increases. There are two different mechanisms that play different roles. One is that, at lower pressures, discharge occurs at higher field magnitudes; according to Ohm's law, at higher field magnitudes, the current density will be higher. A higher current density then leads to a higher discharge

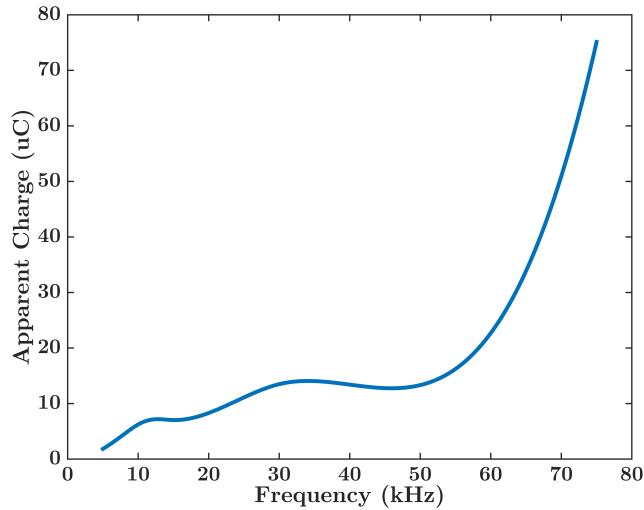


Figure 4.22: The frequency impact on PD inception

magnitude. On the other hand, the relative permittivity declines at lower pressures, which means that the field displacement would be lower ($D = \epsilon E$). Since the field displacement has a direct relationship with the true charge magnitude, at a lower permittivity the amount of true charge would be lower. The variations of relative permittivity at low pressures are not as sharp as at high pressures; hence, the overall increased magnitude of true charge is due to the deeper impact of E_{inc} enhancement versus ϵ_r reduction at low pressures.

4.7 Key Challenges

4.7.1 Estimation of Model Parameters

Choosing proper values for physical parameters is a major duty in PD modeling. To achieve so, the parameters should be estimated such that the model results meet the experimental data.

Each parameter might take part in several characteristics of a discharge including but limiting

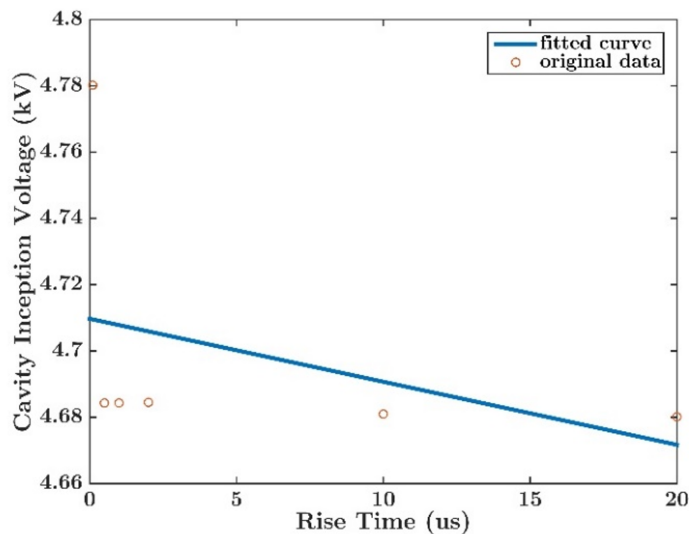


Figure 4.23: The impact of cavity shape on PD charge magnitude

to inception criterion, charge magnitudes, PD duration. For instance, in the 2nd case study, [62] is used to calibrate the parameters. are utilized for the purpose of parameter estimation. The parameters will be adjusted to obtain a similar PRPD pattern. The indices used for calibration specify the freedom degrees. In this regard $\sigma_{cav,max}$, E_{inc} , (E_{ext}), and τ_{dec} selected for the above purpose. $\sigma_{cav,max}$ participate in the adjustment of PD magnitude and duration. The discharge quenches faster if $\sigma_{cav,max}$ is higher; on the other hand, current density has an opposite relationship with $\sigma_{cav,max}$.

E_{inc} controls the time at which PD ignites. In [62], PD inception voltage is reported as $9.5kV$, therefore, the inception field used in our study is the field at which the voltage reaches the above value. The extinction field can also make an impact on the duration of PD as well as its intensity.

Lastly, the time constant is used to handle the PD inception time. By choosing a higher time constant, the availability of initial electron becomes more probable.

The degrees of freedom are used in a way that the mean true charge, the ratio of PD repetition in each half cycle, and the inception voltage meet the experimental results.

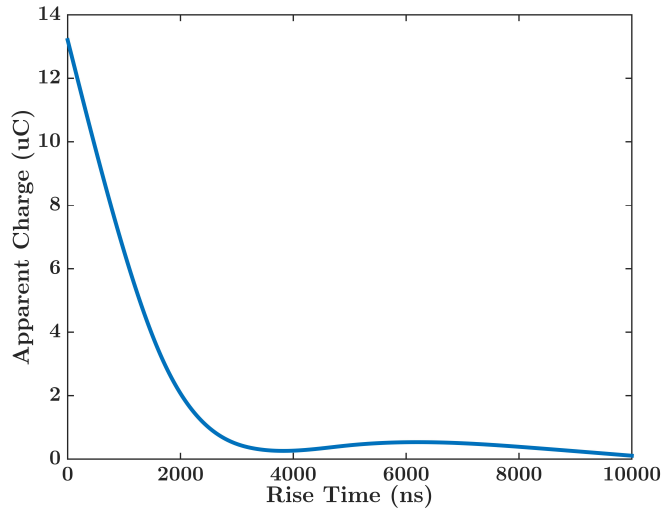


Figure 4.24: The impact of cavity shape on PD charge magnitude

The parameters' values mentioned at the beginning of the this chapter are chosen in accordance with this calibration technique. Fig. 4.29 shows the PRPD pattern for 50 cycles of sine voltage that is in good agreement with the pattern in [62].

4.7.2 Convergence Problem

In the proposed model, the time steps have to be utterly specified by the algorithm. However, the strict time stepping might arise some issues for the convergence.

To prevent any convergence problem, various techniques can be helpful. Using a finer mesh quality with smaller elements, especially at those areas that the electric field is extremely inhomogeneous, could increase convergence probability. Another way to respond to this issue is using a time-stepping method called *generalized- α* . The method, being first applied to structural dynamics problem [74], is an implicit technique used for transient problems and takes over damping degree ($0 < \xi < 1$) at high frequency without substantial impact on the precision. In spite of its accuracy, its instability compared to Backward Differentiation

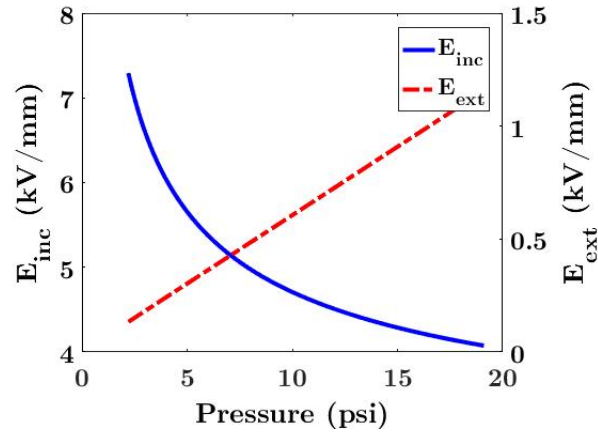


Figure 4.25: Impact of pressure on inception and extinction electric field.

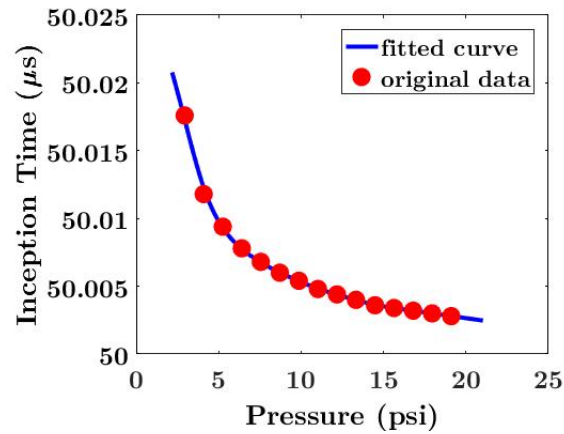


Figure 4.26: PD inception time as a function of pressure.

Formula (BDF) is a disadvantage.

4.7.3 Burden of Calculation

As one could comprehend so far, PD activities are influenced by previous discharges. This can make the modeling of PD phenomenon intricate as a single PD cannot be examined solely.

The accumulation of PD historical data over the time can cause the growth of calculation

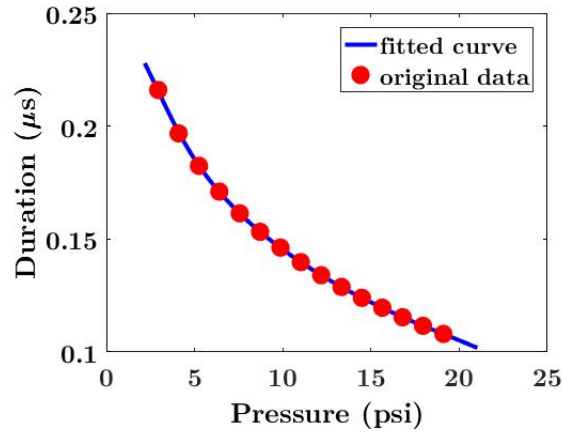


Figure 4.27: The relation between pressure and PD duration.

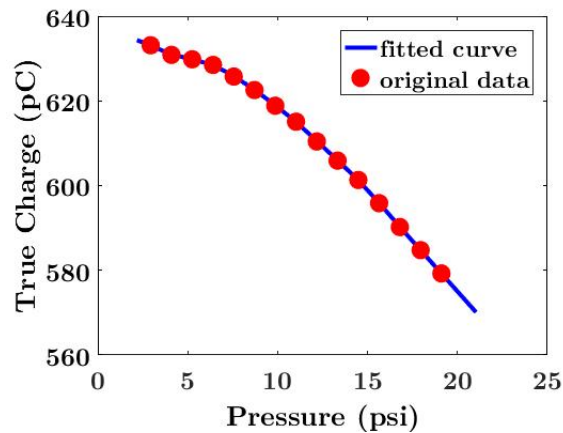


Figure 4.28: The PD charge magnitude versus pressure.

burden as the time goes on. To make the model less time-consuming, a compaction technique might be found handy in order to shrink the burden.

A discharge affects the upcoming PDs in two ways: (1) in the proper model voltage and field distribution, (2) in the surface emission of electrons for the next discharges. The latter makes a deep impact as it specifies the statistical time lag for the next PD event.

To show the contribution of a previous discharge, it is not mandatory to include all the time sets associated with that event; in other words, a few number of time instant can validly approximate the main moments of a discharge. Therefore, N_{comp} is proposed as a number

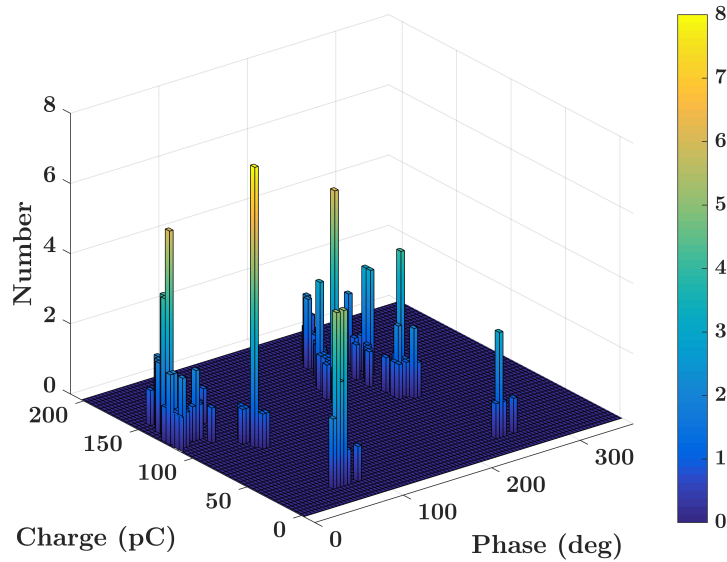


Figure 4.29: The 3D PRPD Pattern for the case study after 50 cycles.

(lower than the total number of time instants) to compactly represent previous PD events.

Fig. 4.29 shows the impact of the compaction technique ($N_{comp} = 20$) on computation time comparing it to the exhaustive modeling of all PD events. The simulations are conducted using a computer system with a processor operating at 3.1 MHz with a RAM memory of 24 GBs.

4.7.4 Dielectric Constant (relative permittivity)

As this study strives to model partial discharge throughout changes in pressure magnitude, it is crucial to take into account the effect of pressure on relative permittivity. The reason for this is that the dielectric constant can change the magnitude of the electric field according to the Maxwell equation and PD modeling is strongly dependent upon the accurate estimation of electric field distribution. Owen and Brinkley suggested that the relative permittivity of

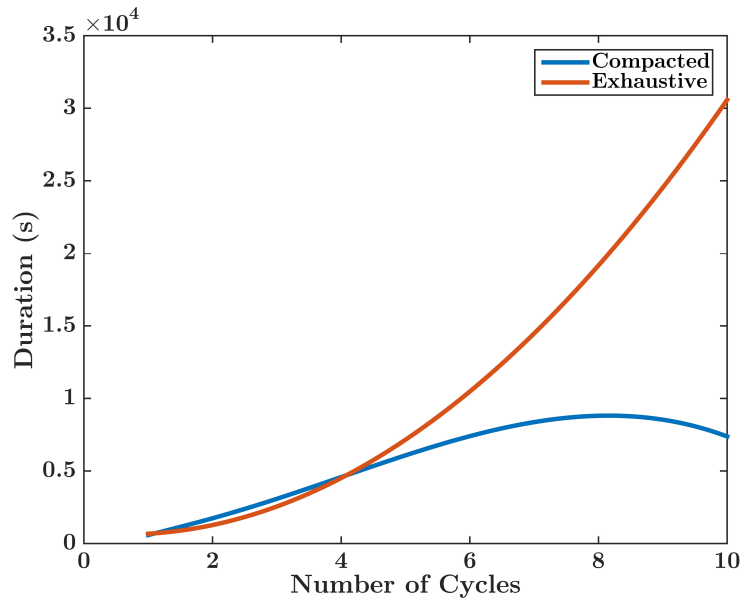


Figure 4.30: The impact of compaction technique on calculation burden.

a dielectric liquid can be given by [75]:

$$1 - \frac{\epsilon_{p_0}}{\epsilon_p} = A \ln\left(\frac{B + p}{B + p_0}\right) \quad (4.1)$$

where ϵ_{p_0} and p_0 denote the relative permittivity and pressure, respectively, under NTP conditions. Similarly, ϵ_p stands for the relative permittivity at pressure p . A and B are constants of Tait expression related to the material and must be experimentally determined. Thus, in this study, approximate values are derived from [75].

To the best of our knowledge, the relative permittivity of gels as a function of pressure has not researched to date. Since silicone gel has properties of dielectric liquids, in this study, we assume that (3) can be used for silicone gel as well. In this regard, Fig. 4.31 shows the changes in silicone gel relative permittivity as a function of pressure. Generally, the figure implies that the relative permittivity has a direct relationship with pressure; however, the rate of change declines as pressure is reduced and ϵ_r has little variations for $p < 1 \text{ atm}$.

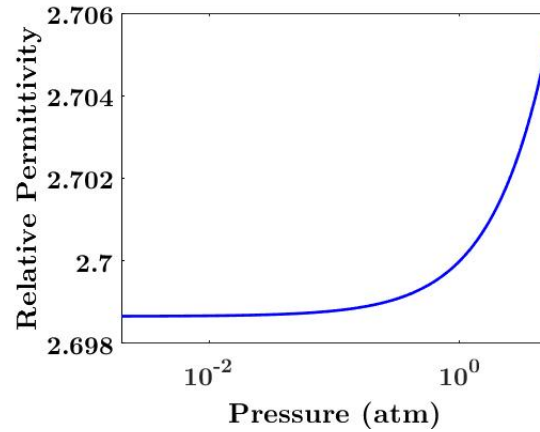


Figure 4.31: The variations of relative permittivity with pressure.

4.8 Summary

The utilization of WBG-based power modules can impose further threats to the insulation systems due to their operation at a higher frequency and higher slew rate. To accurately assess the insulation lifetime of WBG-based power electronics modules under square wave voltages, this study focused on electric field analysis when the dielectric material undergoes a repetitive pulse voltage. To do so, the finite element method was adopted to find the voltage and field distribution within the void-dielectric system. As it was expected, the first PD event occurred at the rising flank of the first voltage pulse, and it was observed that discharge significantly affect the stress on the cavity and its surroundings in a PD event. Also, it was inferred that as the frequency of pulses goes up, the voltage at which PD occurs will be decreased, and larger cavity diameters can give rise to even lower strength.

Considering the fact that the pressure at higher altitudes can be extremely low, this study examined the impact of high frequency, high slew rate unipolar square wave voltage under low-pressure conditions. It was shown that low-pressure conditions have a game-changing impact by influencing the PD inception and extinction times, duration, and intensity. The utilization of WBG-based power modules can impose further threats to the insulation systems

due to their operation at a higher frequency and higher slew rate. Considering the fact that the pressure at higher altitudes can be extremely low, this study examined the impact of high frequency, high slew rate unipolar square wave voltage under low-pressure conditions. It was shown that low-pressure conditions have a game-changing impact by influencing the PD inception and extinction times, duration, and intensity.

Chapter 5

Conclusions

5.1 Discussion and Inference

The growing trend toward the electrification of the aviation industry urges the demand for ensuring the reliability of the insulation system. The crucial role of power electronics in the future needs the examination of power modules from different perspectives to ensure the proper operation of the system. As the new generations of modules benefit from WBG semiconductors, operating at higher voltages, frequencies, and temperatures, it is necessary to scrutinize the electric stress supported by the insulation system. This study, using a modeling approach with the aid of simulation tools, probed into a destructive phenomenon, named PD, that can happen inside the power module.

In this project, a PD model was proposed based on the physical processes taking place during PD phenomena. The model was adjusted to the experimental results reported in the literature. From the obtained results, it is quite obvious that the frequency and rise-time can have a destructive impact on the health of the dielectric. The novel modeling approach proposed in this study, which is done for the first time in the case of fast-rise, high-frequency square voltage, can be a groundwork for any power electronic module design to ensure its reliable operation from the standpoint of insulation performance.

Using the model developed with the aid of COMSOL Multiphysics and MATLAB, the impact

of several parameters such as cavity diameter, cavity shape, cavity location, and square wave rise-time was assessed. It was concluded that all the aforementioned cavity-related parameters could have a significant impact on inception voltage. An increase in the cavity diameter and displacement of the cavity from the center of dielectric toward the sides of the dielectric medium can increase the inception voltage. It was also inferred that by the enhancement of rise-time, PD occurs at a lower voltage across the cavity.

The results have also shown that PD variation causes changes in the inception and extinction of electric fields as well as the relative permittivity of the insulation medium. The results show that despite a slight delay in PD initiation under low-pressure conditions, the true charge magnitude is increased by about 20% and the duration of PD events is nearly doubled at cruise altitude compared to the ground level. As the material's nature has a substantial impact on the extent and nature of the aforementioned changes, more research on different insulating materials can lead to the development of a more reliable insulation system under extremely low-pressure conditions.

5.2 Future Works

An adventure in the development of PD model is the re-investigation of the PD initiation mechanisms from quantum physics point of view. The studies that provide the groundwork for initial electron generation approximation are fairly old, and the difficulty of experimentation in this field has led to some empirical formula fitted to experimental data which is not the most solid way to approximate initial electron generation. However, the availability of new technologies in quantum physics, can provide the opportunity for collaboration to re-investigate the mechanism and sources of electron generation. This study is extremely important due to the impact of PD inception on the intensity of PD and subsequently the

lifetime of dielectric.

The path of evolution for PD modeling includes the two areas discussed above but is not limited to them. PD phenomenon is an interdisciplinary field which has a lot to do with material science and a comprehensive study for future solution to the accelerated aging of insulation systems should work along material science.

Bibliography

- [1] R. Arora and W. Mosch, *High Voltage and Electrical Insulation Engineering*. IEEE Press Series on Power Engineering Series, Wiley, 2011.
- [2] C. M. Martinez, X. Hu, D. Cao, E. Velenis, B. Gao, and M. Wellers, “Energy management in plug-in hybrid electric vehicles: Recent progress and a connected vehicles perspective,” *IEEE Transactions on Vehicular Technology*, vol. 66, no. 6, pp. 4534–4549, June 2017.
- [3] T. Mai, D. Steinberg, J. Logan, D. Bielen, K. Eurek, and C. McMillan, “An electrified future: Initial scenarios and future research for u.s. energy and electricity systems,” *IEEE Power and Energy Magazine*, vol. 16, no. 4, pp. 34–47, July 2018.
- [4] Advisory Council for Aeronautics Research in Europe, *Aeronautics and Air Transport: Beyond Vision 2020 (towards 2050)*. Europ. Comm., Directorate-General for Resaearch Aeronautics and Air Transport, 2010. [Online]. Available: <https://books.google.com/books?id=7ZYgmwEACAAJ>
- [5] —, *Strategic research innovation agenda-2017 update*. Europ. Comm., Directorate-General for Resaearch Aeronautics and Air Transport, 2017. [Online]. Available: <https://books.google.com/books?id=7ZYgmwEACAAJ>
- [6] United States Environmental Protection Agency (EPA), *Fast Facts on Transportation Greenhouse Gas Emissions*, June 2019. [Online]. Available: <https://www.epa.gov/greenvehicles/fast-facts-transportation-greenhouse-gas-emissions>
- [7] United States Energy Information Administration (EIA), “Monthly energy review,”

- Feb 2020. [Online]. Available: https://www.eia.gov/totalenergy/data/monthly/pdf/sec3_9.pdf
- [8] U.S. Department of Energy, Electricity Delivery and Energy Reliability, “Power electronics research and development program plan,” April 2011.
- [9] B. K. Bose, “Power electronics, smart grid, and renewable energy systems,” *Proceedings of the IEEE*, vol. 105, no. 11, pp. 2011–2018, Nov 2017.
- [10] T. Foulkes, J. Oh, R. Pilawa-Podgurski, and N. Miljkovic, “Self-assembled liquid bridge confined boiling on nanoengineered surfaces,” *International Journal of Heat and Mass Transfer*, vol. 133, pp. 1154–1164, Apr. 2019. [Online]. Available: <http://www.sciencedirect.com/science/article/pii/S0017931018351408>
- [11] J. G. Kassakian and T. M. Jahns, “Evolving and emerging applications of power electronics in systems,” *IEEE Journal of Emerging and Selected Topics in Power Electronics*, vol. 1, no. 2, pp. 47–58, June 2013.
- [12] B. M. Grainger, G. F. Reed, A. R. Sparacino, and P. T. Lewis, “Power electronics for grid-scale energy storage,” *Proceedings of the IEEE*, vol. 102, no. 6, pp. 1000–1013, June 2014.
- [13] M. G. Molina, “Energy storage and power electronics technologies: A strong combination to empower the transformation to the smart grid,” *Proceedings of the IEEE*, vol. 105, no. 11, pp. 2191–2219, Nov 2017.
- [14] B. Wang, S. Dong, S. Jiang, C. He, J. Hu, H. Ye, and X. Ding, “A comparative study on the switching performance of gan and si power devices for bipolar complementary modulated converter legs,” *Energies*, vol. 12, p. 1146, 03 2019.

- [15] T.-K. Kim, “A Study on Improving Switching Characteristics According to a Circuit Analysis Technique in Converter Applications Using Gallium Nitride Field Effect Transistors,” *Energies*, vol. 12, no. 17, pp. 1–20, August 2019. [Online]. Available: <https://ideas.repec.org/a/gam/jeners/v12y2019i17p3280-d261083.html>
- [16] A. Fayyaz, G. Romano, J. Urresti, M. Riccio, A. Castellazzi, A. Irace, and N. Wright, “A Comprehensive Study on the Avalanche Breakdown Robustness of Silicon Carbide Power MOSFETs,” *Energies*, vol. 10, no. 4, pp. 1–15, April 2017. [Online]. Available: <https://ideas.repec.org/a/gam/jeners/v10y2017i4p452-d94711.html>
- [17] T. Guillod, R. Faerber, D. Rothmund, F. Krismer, C. M. Franck, and J. W. Kolar, “Dielectric losses in dry-type insulation of medium-voltage power electronic converters,” *IEEE Journal of Emerging and Selected Topics in Power Electronics*, 2019.
- [18] D. Fabiani, *Accelerated Degradation of AC Motor Insulation due to Voltage Waveforms Generated by Adjustable Speed Drives*, Jan. 2003.
- [19] M. Ghassemi, “Electrical insulation weaknesses in wide bandgap devices,” *IntechOpen*, pp. 129–149, Oct. 2018.
- [20] M. Ghassemi, “Accelerated insulation aging due to fast, repetitive voltages: A review identifying challenges and future research needs,” *IEEE Transactions on Dielectrics and Electrical Insulation*, vol. 26, no. 5, pp. 1558–1568, Oct 2019.
- [21] F. H. Kreuger, *Partial Discharge Detection in High Voltage Equipment*. Butterworth-Heinemann, 1990.
- [22] S. A. Boggs, “Partial discharge. iii. cavity-induced pd in solid dielectrics,” *IEEE Electrical Insulation Magazine*, vol. 6, no. 6, pp. 11–16, Nov 1990.

- [23] U. F. Khan, P. I. Lazaridis, H. Mohamed, R. A. Sánchez, Z. D. Zaharis, R. C. Atkinson, C. Tachtatzis, and I. A. Glover, “An efficient algorithm for partial discharge localization in high-voltage systems using received signal strength,” *Sensors*, 2018.
- [24] R. A. Sánchez, J. Ardila-Rey, and A. A. Mas’ud, “On the use of monopole antennas for determining the effect of the enclosure of a power transformer tank in partial discharges electromagnetic propagation,” *Sensors*, vol. 16 2, p. 148, 2016.
- [25] H. Janani, B. Kordi, and M. J. Jozani, “Classification of simultaneous multiple partial discharge sources based on probabilistic interpretation using a two-step logistic regression algorithm,” *IEEE Transactions on Dielectrics and Electrical Insulation*, vol. 24, pp. 54–65, 2017.
- [26] R. J. Densley, “Partial discharges in electrical insulation under combined alternating and impulse stresses,” *IEEE Transactions on Electrical Insulation*, vol. EI-5, pp. 96–103, 1970.
- [27] D. A. Nattrass, “Partial discharge. xvii. the early history of partial discharge research,” *IEEE Electrical Insulation Magazine*, vol. 9, pp. 27–31, 1993.
- [28] B. M. Weedy, S. H. Shaikh, and S. G. Swingler, “Partial discharges in cavities in insulation impregnated with supercritical helium,” *IEEE Transactions on Electrical Insulation*, vol. EI-17, pp. 46–52, 1982.
- [29] R. Bartnikas, “Partial discharges. their mechanism, detection and measurement,” *IEEE Transactions on Dielectrics and Electrical Insulation*, vol. 9, no. 5, pp. 763–808, Oct 2002.
- [30] T. G. Do, O. Lesaint, and J. Auge, “Streamers and partial discharge mechanisms in

- silicone gel under impulse and ac voltages,” *IEEE Transactions on Dielectrics and Electrical Insulation*, vol. 15, 2008.
- [31] G. C. Stevens, E. Perkins, and J. V. Champion, “Microvoid formation and growth in epoxy resins under mechanical and electrical stress by laser light scattering,” in *1988 Fifth International Conference on Dielectric Materials, Measurements and Applications*, June 1988, pp. 234–237.
- [32] S. J. Dodd, L. M. Salvatierra, L. A. Dissado, and E. Mola, “Electrical trees in silicone gel: A combination of liquid and solid behaviour patterns,” *2013 Annual Report Conference on Electrical Insulation and Dielectric Phenomena*, pp. 1018–1021, 2013.
- [33] N. Wang, I. Cotton, J. W. Robertson, S. Follmann, K. Evans, and D. Newcombe, “Partial discharge control in a power electronic module using high permittivity non-linear dielectrics,” *IEEE Transactions on Dielectrics and Electrical Insulation*, vol. 17, 2010.
- [34] L. Niemeyer, “A generalized approach to partial discharge modeling,” *IEEE Transactions on Dielectrics and Electrical Insulation*, vol. 2, no. 4, pp. 510–528, Aug 1995.
- [35] M. Ghassemi, “Pd measurements, failure analysis, and control in high-power igbt modules,” *High Voltage*, vol. 3, no. 3, pp. 170–178, 2018.
- [36] M. Ghessemi, “Geometrical techniques for electric field control in (ultra) wide bandgap power electronics modules,” in *2018 IEEE Electrical Insulation Conference (EIC)*, June 2018, pp. 589–592.
- [37] M. M. Tousi and M. Ghassemi, “Electric field control by nonlinear field dependent conductivity dielectrics characterization for high voltage power module packaging,” *2019 IEEE International Workshop on Integrated Power Packaging (IWIPP)*, pp. 54–58, 2019.

- [38] —, “Nonlinear resistive electric field grading in high-voltage, high-power wide bandgap power module packaging,” *2019 IEEE Energy Conversion Congress and Exposition (ECCE)*, pp. 7124–7129, 2019.
- [39] —, “The effect of type of voltage (sinusoidal and square waveform) and the frequency on the performance of nonlinear field-dependent conductivity coatings for electric field control in power electronic modules,” October 2019.
- [40] I. Laird, X. Yuan, J. Scoltock, and A. J. Forsyth, “A design optimization tool for maximizing the power density of 3-phase dc–ac converters using silicon carbide (sic) devices,” *IEEE Transactions on Power Electronics*, vol. 33, pp. 2913–2932, 2018.
- [41] H. A. Mantooth, M. D. Glover, and P. D. Shepherd, “Wide bandgap technologies and their implications on miniaturizing power electronic systems,” *IEEE Journal of Emerging and Selected Topics in Power Electronics*, vol. 2, pp. 374–385, 2014.
- [42] R. Bosshard and J. W. Kolar, “Inductive power transfer for electric vehicle charging: Technical challenges and tradeoffs,” *IEEE Power Electronics Magazine*, vol. 3, pp. 22–30, 2016.
- [43] P. Wang, A. Cavallini, G. C. Montanari, and G. Wu, “Effect of rise time on pd pulse features under repetitive square wave voltages,” *IEEE Transactions on Dielectrics and Electrical Insulation*, vol. 20, pp. 245–254, 2013.
- [44] G. Finis, A. Claudi, and G. G. Malin, “Dielectric breakdown strength of silicone gel under various environmental conditions,” *2005 IEEE Russia Power Tech*, pp. 1–6, 2005.
- [45] M. Borghei and M. Ghassemi, “Partial discharge finite element analysis under fast, repetitive voltage pulses,” *2019 IEEE Electric Ship Technologies Symposium (ESTS)*, pp. 324–328, 2019.

- [46] —, “Partial discharge analysis under high-frequency, fast-rise square wave voltages in silicone gel: A modeling approach,” *Energies*, vol. 12, no. 23, 2019. [Online]. Available: <https://www.mdpi.com/1996-1073/12/23/4543>
- [47] P. Wang, A. Cavallini, and G. C. Montanari, “The influence of repetitive square wave voltage parameters on enameled wire endurance,” *IEEE Transactions on Dielectrics and Electrical Insulation*, vol. 21, pp. 1276–1284, 2014.
- [48] S. Whitehead, *Dielectric Breakdown in Solids*. Clarendon Press Oxford, 1951.
- [49] G. C. Crichton, P. W. Karlsson, and A. Pedersen, “Partial discharges in ellipsoidal and spheroidal voids,” *IEEE Transactions on Electrical Insulation*, vol. 24, no. 2, pp. 335–342, April 1989.
- [50] A. Pedersen, G. C. Crichton, and I. W. McAllister, “The theory and measurement of partial discharge transients,” *IEEE Transactions on Electrical Insulation*, vol. 26, no. 3, pp. 487–497, June 1991.
- [51] —, “The functional relation between partial discharges and induced charge,” *IEEE Transactions on Dielectrics and Electrical Insulation*, vol. 2, no. 4, pp. 535–543, Aug 1995.
- [52] F. Gutfleisch and L. Niemeyer, “Measurement and simulation of pd in epoxy voids,” *IEEE Transactions on Dielectrics and Electrical Insulation*, vol. 2, no. 5, pp. 729–743, Oct 1995.
- [53] Z. Achillides, M. G. Danikas, and E. Kyriakides, “Partial discharge modeling and induced charge concept: Comments and criticism of pedersen’s model and associated measured transients,” *IEEE Transactions on Dielectrics and Electrical Insulation*, vol. 24, pp. 1118–1122, 2017.

- [54] Z. Achillides, E. Kyriakides, and G. E. Georghiou, "Partial discharge modeling: an improved capacitive model and associated transients along medium voltage distribution cables," *IEEE Transactions on Dielectrics and Electrical Insulation*, vol. 20, pp. 770–781, 2013.
- [55] M. G. Moein Borghei, "Finite element modeling of partial discharge activity within a spherical cavity in a solid dielectric material under fast, repetitive voltage pulses," *IEEE Electrical Insulation Conference (EIC)*, June 2019.
- [56] D. R. Meyer, A. Cavallini, L. Lusuardi, D. Barater, G. Pietrini, and A. Soldati, "Influence of impulse voltage repetition frequency on rpdv in partial vacuum," *IEEE Transactions on Dielectrics and Electrical Insulation*, vol. 25, pp. 873–882, 2018.
- [57] G. Callender, T. Tanmaneeprasert, and P. L. Lewin, "Simulating partial discharge activity in a cylindrical void using a model of plasma dynamics," *Journal of Physics D: Applied Physics*, vol. 52, no. 5, p. 055206, nov 2018. [Online]. Available: <https://doi.org/10.1088%2F1361-6463%2Faaedf0>
- [58] G. Callender, I. O. Golosnoy, P. Rapisarda, and P. L. Lewin, "Critical analysis of partial discharge dynamics in air filled spherical voids," *Journal of Physics D: Applied Physics*, vol. 51, no. 12, p. 125601, feb 2018. [Online]. Available: <https://doi.org/10.1088%2F1361-6463%2Faaae7c>
- [59] E. Kuffel, W. Zaengl, and J. Kuffel, "High voltage engineering fundamentals," *Oxford: Newnes, Second Edition*, 2000.
- [60] G. Finis and A. Claudi, "On the dielectric breakdown behavior of silicone gel under various stress conditions," *IEEE Transactions on Dielectrics and Electrical Insulation*, vol. 14, 2007.

- [61] B. Du, T. Han, and J. Su, "Electrical tree characteristics in silicone rubber under repetitive pulse voltage," *IEEE Transactions on Dielectrics and Electrical Insulation*, vol. 22, pp. 720–727, 2015.
- [62] T. Ebke, A. Khaddour, and D. Peier, "Degradation of silicone gel by partial discharges due to different defects," in *2000 Eighth International Conference on Dielectric Materials, Measurements and Applications (IEE Conf. Publ. No. 473)*, Sep. 2000, pp. 202–207.
- [63] M. Sato, A. Kumada, K. Hidaka, K. Yamashiro, Y. Hayase, and T. Takano, "Surface discharges in silicone gel on aln substrate," *IEEE Transactions on Dielectrics and Electrical Insulation*, vol. 23, pp. 494–500, 2016.
- [64] H. A. Illias, G. Y. Chen, and P. L. Lewin, "Partial discharge behavior within a spherical cavity in a solid dielectric material as a function of frequency and amplitude of the applied voltage," *IEEE Transactions on Dielectrics and Electrical Insulation*, vol. 18, 2011.
- [65] C. Forssén and H. Edin, "Partial discharges in a cavity at variable applied frequency part 2: measurements and modeling," *IEEE Transactions on Dielectrics and Electrical Insulation*, vol. 15, 2008.
- [66] I. Gallimberti, "The mechanism of the long spark formation," *Journal de Physique Colloques*, vol. 40, no. C7, pp. C7–193–C7–250, 1979. [Online]. Available: <https://hal.archives-ouvertes.fr/jpa-00219444>
- [67] H. A. Illias, G. G. Chen, and P. L. Lewin, "Comparison between three-capacitance, analytical-based and finite element analysis partial discharge models in condition monitoring," *IEEE Transactions on Dielectrics and Electrical Insulation*, vol. 24, pp. 99–109, 2017.

- [68] C. Forssen, "Partial discharges in cylindrical cavities at variable frequency of the applied voltage," *Licentiate thesis, Royal Inst. Technol. (KTH), Stockholm, Sweden*, 2005.
- [69] H. A. Illias, G. Y. Chen, and P. L. Lewin, "Modeling of partial discharge activity in spherical cavities within a dielectric material," *IEEE Electrical Insulation Magazine*, vol. 27, 2011.
- [70] R. Schifani, R. Candela, and P. Romano, "On pd mechanisms at high temperature in voids included in an epoxy resin," *IEEE Transactions on Dielectrics and Electrical Insulation*, vol. 8, no. 4, pp. 589–597, Aug 2001.
- [71] H. A. Illias, G. Chen, and P. L. Lewin, "The influence of spherical cavity surface charge distribution on the sequence of partial discharge events," vol. 44, no. 24, p. 245202, jun 2011. [Online]. Available: <https://doi.org/10.1088%2F0022-3727%2F44%2F24%2F245202>
- [72] S. Matsumura and S. Chen, "Effect of plasma resistance on electron temperature measurement by means of an electrostatic probe," *Journal of Applied Physics*, vol. 43, no. 8, pp. 3357–3361, 1972.
- [73] H. A. Illias, G. Chen, and P. L. Lewin, "Partial discharge within a spherical cavity in a dielectric material as a function of cavity size and material temperature," *IET Science, Measurement Technology*, vol. 6, no. 2, pp. 52–62, March 2012.
- [74] J. Chung and G. M. Hulbert, "A Time Integration Algorithm for Structural Dynamics With Improved Numerical Dissipation: The Generalized- Method," *Journal of Applied Mechanics*, vol. 60, no. 2, pp. 371–375, June. 1993.
- [75] L. G. Schornack and C. A. Eckert, "Effect of pressure on the density and dielectric constant of polar solvents," *The Journal of Physical Chemistry*, vol. 74, no. 15,

pp. 3014–3020, Jul. 1970, publisher: American Chemical Society. [Online]. Available:
<https://doi.org/10.1021/j100709a030>